ResearchOnline@JCU

JAMES COOK UNIVERSITY AUSTRALIA

This is the author-created version of the following work:

Sadat-Noori, Mahmood, Maher, Damien T., and Santos, Isaac R. (2016) ***Groundwater Discharge as a Source of Dissolved Carbon and Greenhouse Gases in a Subtropical Estuary.*** **Estuaries and Coasts, 39 pp. 639-656.**

Access to this file is available from:

https://researchonline.jcu.edu.au/78849/

© Coastal and Estuarine Research Federation 2015

Please refer to the original source for the final version of this work:

https://doi.org/10.1007/s12237%2D015%2D0042%2D4

Groundwater discharge as a source of dissolved carbon and greenhouse gases in a subtropical estuary

Mahmood Sadat-Noori*[1,2], Damien T. Maher[1], Isaac R. Santos[1,2]

[1] School of Environment, Science and Engineering, Southern Cross University, Lismore, NSW 2480, Australia

[2] National Marine Science Centre, Southern Cross University, PO Box 4321, Coffs Harbour, NSW 2450, Australia

*Corresponding author:

M. Sadat-Noori, School of Environment, Science and Engineering, Southern Cross University, PO Box 157 Lismore, NSW 2480, Australia (m.sadatnoori@yahoo.com)

Running head: Groundwater influence on carbon cycling

Abstract

Groundwater may be highly enriched in dissolved carbon species, but its role as a source of carbon to coastal waters is still poorly constrained. Exports of deep and shallow groundwater-derived dissolved carbon species from a small subtropical estuary (Korogoro Creek, Australia, latitude -31.04781°, longitude 153.06492°) were quantified using a radium isotope mass balance model (^{233}Ra and ^{224}Ra, natural groundwater tracers) under two hydrological conditions. In addition, air-water exchange of carbon dioxide and methane in the estuary was estimated. The highest carbon inputs to the estuary were from deep fresh groundwater in the wet season. Most of the dissolved carbon delivered by groundwater and exported from the estuary to the coastal ocean was in the form of dissolved inorganic carbon (DIC; 687 mmol m^{-2} estuary d^{-1}; 20 mmol m^{-2} catchment d^{-1}, respectively), with a large export of alkalinity (23 mmol m^{-2} catchment d^{-1}). Average water to air flux of CO_2 (869 mmol m^{-2} d^{-1}) and CH_4 (26 mmol m^{-2} d^{-1}) were 5 and 43 fold higher, respectively, than the average global evasion in estuaries due to the large input of CO_2 and CH_4 enriched groundwater. The groundwater discharge contribution to carbon exports from the estuary for DIC, dissolved organic carbon (DOC), alkalinity, CO_2 and CH_4 was 22%, 41%, 3%, 75% and 100%, respectively. The results show that CO_2 and CH_4 evasion rates from small subtropical estuaries surrounded by wetlands can be extremely high, and that groundwater discharge had a major role in carbon export and evasion from the estuary and therefore should be accounted for in coastal carbon budgets.

Key words: Submarine groundwater discharge, surface water- groundwater interaction, Carbon dioxide, methane, permeable sediments, radon, cavity ring down spectrometry, mangrove, greenhouse gases.

1. Introduction

Estuarine ecosystems provide a major pathway for carbon to travel across the land–ocean interface and are considered an important component of the global carbon cycle (Rodríguez-Murillo et al. 2015; Seitzinger et al. 2005). Estuarine carbon input and transformation processes include material exchange with surrounding environments (Hans et al. 2011) (in particular coastal wetlands (Cai 2011)), high rates of primary productivity and respiration (Bianchi 2007), benthic-pelagic coupling (Maher and Eyre 2010), freshwater inputs (Dixon et al. 2014), atmospheric exchange (Borges and Abril 2011) and groundwater discharge (Liu et al. 2014). Of these processes, groundwater exchange is probably the most poorly resolved and has received little attention until recently.

Groundwater discharge/porewater exchange has been suggested to influence carbon cycling in estuarine environments (Santos et al. 2012a; Faber et al. 2014; Wang et al. 2015). Groundwater inputs to coastal waters may be volumetrically small when compared to surface water inputs, however, due to the high concentrations of dissolved constituents, groundwater can be a major pathway for dissolved material exports between terrestrial and coastal systems (Burnett et al. 2006; Maher et al. 2013a; Liu et al. 2014). Submarine groundwater discharge (SGD) is defined as the exchange of groundwater between land and ocean regardless of its composition and scale and may be fresh terrestrial, recirculated seawater or a combination of both (Moore 2010). Fresh groundwater delivers new water along with dissolved constituents, while recirculated saline groundwater can deliver large amounts of recycled carbon and nutrients to surface waters (Weinstein et al. 2007; Gleeson et al. 2013; Liu et al. 2014). The fresh and

recirculated marine components of SGD are often well mixed, thus making quantification of their relative contribution to coastal waters complex.

Previous studies exploring SGD inputs of dissolved carbon have reported that groundwater discharge from aquifers to the estuarine and coastal zones, may be a significant source of CO_2 and CH_4 to the atmosphere (Cai 2011; Atkins et al. 2013; Call et al. 2015). Additionally, pCO_2 and CH_4 in groundwater can be orders of magnitude higher than atmospheric values (Gagan et al. 2002; Cai 2003; Call et al. 2015). However, estuarine carbon budgets have rarely assessed the importance of groundwater discharge as a driver of CO_2, dissolved inorganic carbon (DIC) and dissolved organic carbon (DOC). The results from these limited studies clearly demonstrate that groundwater inputs of dissolved carbon can be significant and warrant quantification in coastal carbon budgets (Porubsky et al. 2014; Wang et al. 2015).

Most previous studies related to groundwater-derived carbon cycling, have been conducted in the USA and Australia, however, there is still a lack of data from a variety of ecosystems, including estuaries in the southern hemisphere (Cai 2003; Liu et al. 2012; Maher et al. 2013a). Prior studies have attempted to estimate groundwater-derived fluxes of DIC (Atkins et al. 2013), DOC (Goñi and Gardner 2003; Kim et al. 2011), alkalinity (Steward et al., 2015; Cyronak et al. 2014), DIC and DOC (Santos et al. 2012a; Maher et al. 2013a; Porubsky et al. 2014) or DIC and alkalinity (Santos et al., 2015; Liu et al. 2014; Wang et al. 2015) into coastal waters. To our knowledge, no previous study has attempted to simultaneously quantify groundwater-derived inputs of the four main dissolved carbon species (DIC, DOC, CO_2 and CH_4) and alkalinity into an estuary, and the relative importance of groundwater carbon inputs to atmospheric evasion of CO_2 and CH_4 and carbon exports to the coastal ocean.

We hypothesize that groundwater discharge into a small subtropical estuary will be a significant pathway for carbon exported to the coastal ocean. We tested this hypothesis by performing time series measurements of carbon parameters (DIC, DOC, pCO_2, pCH_4), alkalinity, ^{222}Rn and Ra isotopes in a tidal estuary that has a simple geometry. Our objectives were to (1) estimate atmospheric CO_2 and CH_4 evasion rates from the estuary, (2) calculate groundwater-derived inputs to the estuary of the four main dissolved carbon species and alkalinity under contrasting hydrological conditions (wet season and dry season), (3) quantify the relative importance of meteoric fresh, and recirculated saline groundwater-derived carbon inputs to the estuary, and (4) determine the relative importance of groundwater in the total carbon and alkalinity exports from the estuary to the coastal ocean. This study builds on a companion paper reporting a detailed radon and radium isotope investigation in the same system (Sadat-Noori et al., 2015).

2. Materials and method

2.1. Site description

The investigation was carried out in Korogoro Creek (latitude -31.04781°, longitude 153.06492°), a small (5 km long, ~ 20-25 m wide, average depth 0.9 m, area 116,160 m^2) subtropical tidal estuary in Hat Head, NSW, Australia (Fig. 1). The estuary has a small catchment (18 km^2) which is low lying and subject to flooding by seawater during spring tides. The estuary has a residence time of one day and is normally flushed during each tidal cycle, with ocean water penetrating the lower 4 km of the estuary at high tide (Ruprecht and Timms 2010). The region has an average annual rainfall of 1,490 mm and experiences a mild subtropical

climate all year round. January and July have the highest (26.9°C) and lowest (11.2°C) monthly mean air temperatures, respectively. Rainfall is highest from February to March (175.2 mm month^{-1}) and lowest from July to September (71 mm month^{-1}) (http://www.bom.gov.au). Our most downstream station was located at the mouth of the estuary (153°3'27.268"E; 31°3'24.801"S) at a sandy beach environment, while the rest of the stations were surrounded by fringing mangrove vegetation.

2.2. Experimental design

Two field campaigns were carried out over two seasons (wet and dry). The first set of time series data collection (wet season) was conducted from 08:45 am March 25th to 10:15 am March 27th 2013, while the second field campaign (dry season) was carried out from 20:30 June 6th to 10:00 am June 10th 2013. Both field campaigns were conducted around the spring tides. However, the tidal range between the semi-diurnal tides varied. During the wet season the tidal range was similar between the semi-diurnal tides (~1.2m), while in the dry season the tidal range varied between ~ 0.6 and 1m (Fig. 2) over the semi-diurnal tides.

During the first field campaign, we deployed automatic high frequency time series monitoring stations at four approximately equally spaced sites (~ 1 to 1.5 km apart) along the length of the estuary (Fig. 1). During the second field campaign, two time series monitoring stations were deployed. The station at the mouth of the estuary, here after referred to as "downstream station" continually monitored salinity, temperature, dissolved oxygen, current velocity, pCO_2, pCH_4 and ^{222}Rn, during the two field campaigns, while the other stations measured the same suite of parameters with the exception of pCH_4. A time series of discrete samples for DIC, DOC and TAlk were also collected from the downstream station every hour

over 2 consecutive tidal cycles (> 25 hours) during both sampling campaigns. Groundwater samples were collected throughout the catchment (Fig. 1) by installing shallow piezometers (Charette and Allen, 2006) and by sampling deep monitoring wells in the region to characterise the groundwater endmember concentration. A mass balance model was developed to evaluate fresh and saline groundwater-derived carbon and alkalinity fluxes, atmospheric exchange rates of CO_2 and CH_4, and to quantify carbon exports from the estuary.

2.3. Surface water time series observations

A calibrated Hydrolab automatic logger was used to measure pH (± 0.02 units), salinity (± 0.02 ppt), dissolved oxygen (± 0.2 mg L^{-1}), and water temperature (± 0.10 °C), at 15 min intervals, at all stations, during both sampling campaigns. Depth loggers (CTD divers – Schlumberger Water Services) measured estuary depth (± 0.01 m), at 10 minute intervals at each of the four stations. Wind speed data were obtained online (www.wunderground.com) from a weather station at 10 m height located at South West Rocks, about 15 km away from the study site. An acoustic doppler current profiler (ADCP; Sontek Argonaut) was installed in the middle of the estuary at the downstream site to measure current velocity and direction of flow averaged over 10 min intervals. This was combined with time specific cross sectional area (adjusted for tidal height) to obtain 10 min discharge estimates assuming that currents across the channel were homogenous. At the other three time series stations, current velocity was measured using Starflow Ultrasonic Doppler Flow Recorders. The estuary cross section was measured at high tide using a depth gauge at 2 m width intervals.

For determining ^{222}Rn concentrations, hereafter referred to as “radon”, a radon-in-air monitor modified for radon-in-water (RAD 7, Durridge Co.) was used (Burnett et al. 2010 and

156 references therein). Radon was measured every 10 minutes for about 40 hours in the wet season
157 and 60 hours in the dry season. At the downstream station during both seasons, a cavity ring
158 down spectrometer (Picarro G2201-i) coupled to a showerhead equilibrator was used to measure
159 pCO_2 and pCH_4 at ~ 1 Hz (Maher et al. 2013b) with data averaged over 1 minute intervals. The
160 equilibrated air is continuously pumped in a closed-loop from the headspace of the equilibrator
161 chamber through desiccant (Drierite), the cavity ring down spectrometer, a RAD7 and then back
162 to the equilibrator. For measuring pCO_2 at other stations, a Li-Cor 820 CO_2 analyser coupled to a
163 RAD7 radon monitor was used (Santos et al. 2012b). CH_4 partial pressure was converted to
164 concentrations based on the solubility coefficient calculated as a function of temperature and
165 salinity (Wiesenburg and Guinasso, 1979) to allow for easy comparison with previous studies
166 that generally use CH_4 concentration rather than partial pressure.
167 Discrete samples were collected using a sample-rinsed 60 ml polyethylene syringe every
168 hour for about 25 hours from the downstream station in both seasons. Samples collected for DIC
169 and DOC concentrations were filtered through 0.7 µm Whatman GF/F filters into acid-rinsed,
170 milli-q rinsed, precombusted (4 hours 400ºC) 40 ml volatile organic carbon borosilicate vials
171 containing 100 µl of saturated $HgCl_2$, without any head space or bubbles. Samples for alkalinity
172 (TAlk) were filtered through 0.7 µm Whatman GF/F and collected in 30 ml polycarbonate vials.
173 The samples were stored on ice until returning to the lab where they were stored at 4 ºC until
174 analysis.
175
176 **2.4. Groundwater Sampling**
177 Groundwater sampling was performed at the same time as surface water sampling in both
178 field campaigns. Samples were collected using a push point piezometer system (Charette and

179 Allen 2006). The tubing was thoroughly flushed with the sample prior to collecting each sample.
180 DOC, DIC and TAlk were sampled as per surface water methods described earlier. For radon,
181 shallow wells ranging between 0.5 – 2 m deep were dug adjacent to the estuary near each time
182 series station (Fig. 1), using a hand held auger at low tide. PVC pipes with 50 cm long slotted
183 screens were installed to allow groundwater infiltrate into the pipe. In addition, deep (5 – 21 m)
184 monitoring wells installed by the NSW Office of Water located across the catchment were also
185 sampled (Fig. 1). A peristaltic pump was used to take samples after the wells were purged (3
186 times the casing volume). Groundwater samples are the same as those used for radium isotope
187 and radon concentrations in Sadat-Noori et al. (2015).

188 Samples for CO_2 and CH_4 were collected in gas-tight 250 ml bottles, overflowing at least 3
189 times the bottle volume, to which 200 µL of saturated $HgCl_2$ solution was added. A calibrated
190 handheld YSI multiprobe was used to determine pH, temperature, DO and salinity for each
191 groundwater sample. A total of 27 groundwater samples were collected. Six liter gas-tight HDPE
192 plastic bottles were used to collect samples for groundwater radon analysis. Each 6 liter bottle
193 was connected to a RAD7 radon monitor and given at least 2 hours to achieve an air-water radon
194 equilibrium with <5% uncertainty following well established protocols (Lee and Kim 2006).
195 After radon analysis, the water was filtered through magnesium impregnated acrylic fibers for
196 radium analysis (Peterson et al. 2009). Groundwater samples were classified in two classes; deep
197 (>5 m) and shallow (<5 m) based on the radium data in the companion paper (Sadat-Noori et al.,
198 2015).

199

200 **2.5. Analytical Methods**

Groundwater CO_2 and CH_4 samples were analysed via a headspace method using a Picarro G2201-i as described by Gatland et al. (2014). Analysis for DIC and DOC concentrations were carried out following the wet oxidation method (St-Jean 2003) with an OI Aurora 1030W interfaced with a Therma Delta V+ Isotope Ratio Mass Spectrometer (IRMS) (Maher and Eyre 2011). TAlk, (± 0.2%) was measured by Gran Titration using a Metrohm automatic titrator and 0.01M HCl standardized to Dickson Certified Reference Material (Batch 111). Free CO_2 within the estuary was determined by using the DIC and TAlk pair, and also the pCO_2 and TAlk pair, using version 25 of the CO_2SYS program (Pelletier et al., 2007) with the carbonic acid disassociation constants from Millero et al. (2006) and the $KHSO_4$ constant from Dickson (1990). Radium samples were collected at the downstream time series station every hour for 30 hours in wet and dry seasons and a Radium Delayed Coincidence Counter (RaDeCC) was used for measuring ^{223}Ra and ^{224}Ra based on Moore and Arnold (1996). Radium data and estimated groundwater discharge rates are presented in a companion paper (Sadat-Noori et al., 2015).

2.6. Calculations

The CO_2 and CH_4 atmospheric exchange were estimated following Wanninkhof (1992):

$$\text{Flux} = k\,\alpha\,(C_{water} - C_{air}) \quad (1)$$

where C_{water} and C_{air} are the partial pressure of CO_2 or CH_4 in the water column and in air, respectively, in units of µatm; α is the solubility coefficient, calculated as a function of temperature and salinity using the constants of Weiss (1974) for CO_2 and Wiesenburg and Guinasso, (1979) for CH_4, k is the gas transfer velocity at the water–air boundary (m d^{-1}). The

atmospheric pCO_2 and pCH_4 were assumed to be constant at an average of 400 and 1.8 µatm, respectively. We used an empirical equation which estimates transfer velocity as a function of water depth, current and wind speed, which are the dominant sources of water turbulence in estuarine systems (Borges et al., 2004):

$$k_{600} = 1 + 1.719 W^{0.5} D^{-0.5} + 2.58 U_{10} \quad (2)$$

where k_{600} is the transfer velocity (normalised to a Schmidt number of 600), W is the water current (cm s^{-1}); D is water depth (m) and U_{10} is the wind speed at a height of 10 m (m s^{-1}). The Schmidt number is defined as the ratio between the kinematic viscosity to mass diffusivity. All k_{600} values were corrected for the Schmidt number of CO_2 and CH_4 at in situ temperatures and salinities (Wanninkhof 1992), assuming a linear relationship between salinities of 0 and 35. The main uncertainty associated with quantifying air-water gas exchange results from the estimation of gas transfer velocity (k). Most previous studies have used empirical equations which calculate transfer velocity only as a function of wind speed. The model used in this study incorporates current and wind induced turbulence at the air-water interface.

The hourly estuarine export (ebb tide) and import (flood tide) of the four dissolved carbon species (DIC, DOC, free CO_2 and CH_4) and total alkalinity was estimated by multiplying hourly discharge rates by the carbon species concentration. Daily averages where calculated by integrating export and import rates over 2 tidal cycles then dividing by total time for the 2 tidal cycles (~ 25 hours) to get an hourly rate, and multiplying by 24 (hours in one day) to obtain a daily rate. Groundwater carbon fluxes were calculated by multiplying the corresponding daily

volumetric groundwater discharge in each season obtained from Sadat-Noori et al. (2015) by the median concentration of different carbon species in groundwater following Equation (3):

$$GW_{C\ flux} = GW_{dis} \times GW_{med.\ C\ conc.} \quad (3)$$

where $GW_{C\ flux}$ is groundwater carbon fluxes, GW_{dis} is groundwater discharge in each season and $GW_{med.\ C\ conc.}$ is median concentration of different carbon species in groundwater. The median concentration was used due to the non-normal distribution of the groundwater endmember concentrations.

A non-steady state radium mass balance was applied to quantify fresh and saline discharging groundwater into the estuary. The model details and results are presented in a companion paper (Sadat-Noori et al., 2105). Briefly concentrations of radium in surface water are converted into net fluxes of groundwater, discharging into the estuary over a 24h diel cycle. Inputs to the model were groundwater, upstream ^{223}Ra input flux during flood tide, diffusion from sediments and desorption from suspended sediments while outputs consisted of ^{223}Ra downstream output flux during ebb tides and the ^{223}Ra decay.

3. Results

3.1. Hydrological conditions

Contrasting hydrological conditions occurred during each field campaign. Two months prior to the time series measurements in the March (wet season) the area received 612 mm of rainfall. The June 2013 (dry season) time series deployment had base flow conditions with only 57 mm of

rain in the two months prior to field campaign. As a result, the groundwater level during March was 100 cm higher than in June. Based on the rainfall events of the area and for simplicity, we describe the first and second field campaigns as wet and dry seasons respectively. Surface freshwater discharge (i.e. net freshwater discharge out of the mouth of the estuary) was 3 m^3 s^{-1} in the wet season and decreased to 2.2 m^3 s^{-1} in the dry season. Wet season had an average surface water temperature of 25.9 ºC compared to 19.4 ºC in the dry season. Wind speeds were on average 3.1 and 1.7 m s^{-1} during the wet and dry seasons, respectively (Fig. 2). Tidal range was ~ 1.2 m in the wet season while in the dry season the tidal range varied between 1 m and 0.6 m (Fig. 2). Salinity showed a tidal trend and ranged from nearly fresh (1) to saline (up to 35) over a tidal cycle (Fig. 2). Salinity increased rapidly during the start of the flood tide just taking 2.5 hours to reach 34 and dropped more slowly during ebb tide taking about 5 hours to reach minimum values. Similar salinity trends were observed in both campaigns.

3.2. Groundwater observations and discharge rates

Shallow and deep groundwater dissolved carbon concentrations were highly variable (Table 1). Median DIC, DOC and TAlk in shallow groundwater were 1.1, 1.2 and 1.5 times higher than deep groundwater. Median pCO_2 in deep samples (21,109 µatm) was similar to median pCO_2 in shallow samples (20,924 µatm), while median CH_4 concentration was 6.6 times higher in the deep samples (53 µM) than shallow (8 µM).

The discharging groundwater into the estuary surface water was separated into shallow saline and deep fresh groundwater components. Depth was used as a separation factor rather than salinity because in a tidal estuary with a short resident time salinity may not truly represent the spatial groundwater distribution along the estuary. For example, tidal pumping at the

downstream station would cause high salinities in shallow groundwater, while the salinity in groundwater samples at station 4 were never higher than 5. Moreover, the 5 m indicator used as a separation was based on the fact that radium concentration was generally higher in samples collected below 5 m (see Sadat-Noori et al. 2015).

Separate discharge rates were estimated based on ^{223}Ra and ^{224}Ra for wet and dry seasons and deep and shallow groundwater discharge. An average of the ^{223}Ra and ^{224}Ra rates was used to calculate seasonal deep and shallow groundwater discharge rates which were then used to calculate groundwater-derived carbon fluxes entering estuary surface water (refer to Sadat-Noori et al., 2015 for groundwater discharge calculations). In the wet season, groundwater-derived DIC from fresh deep groundwater was 1.8 times higher than saline shallow groundwater-derived DIC. DOC and alkalinity derived from fresh deep groundwater was 1.7 and 1.3 fold higher than saline shallow groundwater-derived DOC (Table 2). Groundwater-derived free CO_2 and CH_4 were 2.1 and 14 fold higher from fresh deep groundwater compared to shallow. In the dry season, DIC, DOC, alkalinity and free CO_2, from saline shallow GW were 6.2, 6.3, 8.8 and 5.3 times higher than the fresh deep groundwater fluxes while CH_4 fluxes were similar from both deep and shallow fluxes. All estimates of groundwater-derived carbon inputs to the estuary were higher in the wet season (Table 2).

3.3. Estuary surface water time series measurements

Dissolved oxygen (DO) followed a clear tidal trend with the highest values at high tide (Fig. 2). DO reached 100% saturation at high tide in both seasons and dropped to 50 and 30% at low tide during the dry and wet seasons, respectively. Radon, pCO_2 and CH_4 followed a tidal trend in both seasons with the highest concentrations being recorded at low tide and lowest at high tide

315 (Fig. 2). Radon concentrations ranged from 0.6 to 180.2 Bq m^{-3} with an average of 50.5 Bq m^{-3}
316 in wet season and varied between 6.2 to 209.1 Bq m^{-3} with an average of 86.5 Bq m^{-3} in dry
317 season, respectively (Fig. 2).

318 DOC followed a tidal trend with high concentrations at low tide and low concentrations at
319 high tide (Fig. 2), while DIC and TAlk concentrations displayed an opposite tidal trend (high
320 concentrations at high tide). DIC concentrations ranged from 809 to 2,151 µM with an average
321 of 1,558 µM in wet conditions and 1,500 µM in the dry season (Fig. 2). DOC ranged from 38 to
322 2,158 µM with an average of 931 µM in the wet season and 668 µM in the dry season. Alkalinity
323 varied between 840 and 2,347 µM with a similar average in both seasons.

324 Carbon dioxide was the only carbon species with observations in multiple stations along the
325 estuary. At the downstream station, pCO_2 followed a tidal trend and was 1.5 times higher in the
326 wet season compared to the dry season (Fig. 3). Average pCO_2 at stations 2, 3 and 4 was about
327 14,000 µatm in the wet season. Average pCO_2 for station 2 in the dry was 9,549 µatm. Maximum
328 pCO_2 in surface waters was 25,130 µatm in the wet season (station 2) and 16,764 µatm in the dry
329 season (Fig. 3). CH_4 concentrations (station 1 only) ranged from 5 nM (high tide) to about 3 µM
330 (low tide), while in the dry season CH_4 varied between 5 nM (high tide) to 4.8 µM (low tide).
331

332 **3.4. CO_2 and CH_4 water to air fluxes**

333 Stations 1, 2, 3 and 4 had average gas transfer velocities (k_{600}) values of 4.6, 3.0, 4.4 and 3.1
334 m d^{-1} respectively, in the wet season while stations 1 and 2 had k_{600} values of 1.7 and 2.9 m d^{-1},
335 respectively, in the dry season. In the wet season, CO_2 fluxes from the lower, mid and upper
336 estuary were estimated to be 573 (station 1 average), 1505 (average of station 2 and 3) and 1650
337 mmol m^{-2} d^{-1} (average of station 3 and 4), respectively. In the dry season the average was 220 for

338 station 1 and 1300 mmol m^{-2} d^{-1} for station 2 (no upper estuary values in dry season, due to
339 vandalism). Wet and dry seasons had an integrated average CO_2 flux of 1128 and 620 mmol m^{-2}
340 d^{-1} (Table 3). CH_4 fluxes from the downstream station were 17 and 43 mmol m^{-2} d^{-1} in wet and
341 dry seasons respectively (Table 3).
342
343 **3.5. Estuarine carbon export**
344 The Hat Head estuary exported on average 20 ± 4 and 9 ± 2 mmol C m^{-2} of catchment d^{-1} of
345 DIC and DOC, respectively, to the coastal ocean (Table 4) based on the two field campaigns.
346 DIC, DOC, TAlk and free CO_2 exports were 35%, 80%, 30% and 93%, higher in the wet season
347 compared to the dry season, while CH_4 was 50% higher in the dry season. Average alkalinity
348 export (23 ± 5 mmol m^{-2} of catchment d^{-1}), was similar to DIC and ~ 6 times higher than free
349 CO_2 (4 ± 1 mmol C m^{-2} of catchment d^{-1}) and several orders of magnitude higher than CH_4
350 (0.005 ± 0.001 mmol C m^{-2} of catchment d^{-1}).
351
352 # 4. Discussion
353
354 **4.1. Carbon data integrity**
355 As we over constrained the carbonate system we investigate the reliability of our measured DIC
356 data by comparing measured DIC concentrations with those calculated from pCO_2 and TAlk
357 (Fig. 4). Our comparison showed that calculated DIC concentrations were on average 9% higher
358 than measured DIC concentration in 90% of the surface water samples. However, for fresh
359 groundwater DIC samples, calculated and measured concentrations showed a closer agreement
360 (Fig. 4b). The lower measured DIC concentrations may be due to CO_2 losses through contact to

361 air at the time of sampling and filtration, and/or, due to an overestimation of calculated DIC due
362 to the contribution of organic acids to the TAlk pool (Hunt et al., 2011, Abril et al., 2015). In
363 spite of these uncertainties, the estimated estuary DIC export rates are similar using both
364 calculated and measured DIC, with only a 8% and 6% higher export rate using the calculated
365 DIC values in the wet and dry season respectively (Table 4).
366
367 **4.2. Carbon water to air fluxes**
368 Water to air CO_2 and CH_4 fluxes over the study period show that Hat Head estuary was a
369 source of CO_2 (620 to 1128 mmol m^{-2} d^{-1}) and CH_4 to the atmosphere (17 to 43 mmol m^{-2} d^{-1})
370 (Table 3). Atkins et al. (2013) reported similarly high CO_2 fluxes of 800 mmol m^{-2} d^{-1} in the
371 upper North Creek Estuary, NSW, Australia with a smaller *k* value of 2.8 m d^{-1}. Frankignoulle et
372 al. (1998), found that nine European estuaries had a mean CO_2 flux of 170 mmol m^{-2} d^{-1} using a
373 *k* value of 1.9 m d^{-1}. The average CO_2 emission from ten Brazilian estuaries was reported to be
374 55 ± 45 mmol m^{-2} d^{-1} with pCO_2 varying between 168 to 8,638 µatm (Noriega and Araujo 2014).
375 We calculated fluxes based on empirical models of *k* similar to Atkins et al. (2013) and Noriega
376 and Araujo (2014), while Frankignoulle et al. (1998) used the floating chamber method. The
377 global average pCO_2 in upper estuaries is estimated to be 3033 ± 1078 µatm with a
378 corresponding atmospheric CO_2 flux of 188 ± 70 mmol m^{-2} d^{-1} (Chen et al., 2012). In our case,
379 the CO_2 water to air flux from the upper estuary (1650 mmol m^{-2} d^{-1}) was an order of magnitude
380 higher than the estimated global average. The high fluxes in this study are likely to be directly
381 related to groundwater inputs (see below).
382 Several previous studies have utilized a fixed time series measuring station usually located
383 at the mouth of the estuary to estimate CO_2 and/or CH_4 flux for the entire area of the estuary

(Bouillon et al. 2007; Maher et al. 2013a). While time series measurements have the advantage of capturing temporal variation with very high resolution, they may not be representative of estuary-wide fluxes due to the inability to account for spatial variation. Maher et al. (2015) suggested that multiple time series stations or a combination of both time series and survey methods may be required to adequately constrain the variability of estuarine CO_2 and CH_4 fluxes at the estuary scale. Here, we simultaneously deployed four fixed time series stations approximately 1.5 km apart along the length of the estuary (~ 5 km) to cover both temporal and spatial variability, thus providing a more robust estimate of the estuary-wide CO_2 dynamics. A similar sampling strategy could not be applied to CH_4 and other carbon species due to logistic reasons.

Our multi-station approach demonstrated the importance of spatial variability in estuarine pCO_2, when calculating estuary-wide fluxes. We estimated CO_2 fluxes using four automated measuring stations in the wet season and two stations in the dry season. If we would have only used a single station at the mouth of the estuary, CO_2 fluxes upscaled to the entire estuary would be underestimated by 50% and 65% during the wet and dry seasons respectively, (573 and 220 mmol m^{-2} d^{-1}, for wet and dry seasons), however, still an order of magnitude higher than the global average estimate for lower estuaries (19 – 59 mmol m^{-2} d^{-1}) (Borges and Abril 2011; Cai 2011; Chen et al. 2013). This was calculated following equation (1) by assuming that the downstream station represented a partial pressure of CO_2 and k value for the entire estuary (i.e. the downstream flux was applied to the entire estuary area). By using the 4 stations, the estuary could be fragmented, with each section having a site-specific set of partial pressures and piston velocities. On the other hand, if sampling had been conducted only in the upstream section of the estuary, CO_2 fluxes would be overestimated considerably. This clearly demonstrates the

importance of collecting spatial data from the lower, middle and upper parts of estuarine systems to be able to estimate a more realistic water-air flux of CO_2 as suggested by previous studies (Wang and Cai 2004; Cai 2011; Maher et al. 2015).

Average CH_4 fluxes from Hat Head estuary were high, averaging 26 mmol m^{-2} d^{-1} (Table 3). These fluxes are about 43 times higher, than the higher end of average global methane flux estimates, from tidal estuaries, which range between 0.04 – 0.6 mmol m^{-2} d^{-1} (Borges and Abril 2011). Ferrón et al. (2007) and Zhang et al. (2008) reported an annual average CH_4 flux of 0.66 and 0.61 mmol m^{-2} d^{-1} from tidal estuaries in Bay of Cádiz, SW Spain and Changjiang, China, while Nirmal Rajkumar et al. (2008) reported CH_4 fluxes of 3.6 mmol m^{-2} d^{-1} from an estuarine system (Adyar) in India. Maher et al. (2015) found CH_4 fluxes in a subtropical Australian estuary to be 0.57 mmol m^{-2} d^{-1}, Linto et al. (2014) and Call et al. (2015) reported CH_4 fluxes from tidal mangrove estuaries to be 0.35 and 0.21 mmol m^{-2} d^{-1}, respectively.

Average CO_2 atmospheric fluxes were 1.8 times higher in wet (1128 mmol $m^{-2}d^{-1}$) than the dry seasons (620 mmol m^{-2} d^{-1}) (Table 3). This difference may be related to higher temperatures in the wet season (summer) and subsequent higher rates of in situ respiration, and/or nitrification which has a net effect of decreasing alkalinity and pH and therefore increasing pCO_2 (Frankignoulle et al., 1996; Gazeau et al. 2005; Borges and Abril, 2011, Maher and Eyre 2012). Interestingly, water to air CH_4 fluxes where higher in the dry (43 mmol m^{-2} d^{-1}) than the wet season (17 mmol m^{-2} d^{-1}), driven by higher concentrations (Fig. 2) rather than higher transfer velocities (Table 3). This is in spite of higher groundwater inputs in the wet season (Table 2). This may be due to seasonal differences in methane oxidation rate (Abril and Iversen 2002) or alternative sources or production rates of CH_4 within the estuary during the two seasons. Further

studies would be required to assess the factors controlling seasonal variability in surface water CH_4 dynamics.

While CO_2 emissions may dominate carbon gaseous fluxes, CH_4 emissions could have a greater impact on global warming potential of the system (Gatland et al. 2014). Although CH_4 losses to the atmosphere were smaller than CO_2, CH_4 is a more potent greenhouse gas compared to CO_2, therefore, accounting only for CO_2 evasion in systems where there may be high CH_4 emissions, could result in an underestimation, in terms of global warming potential of the system (Gatland et al. 2014; Panneer Selvam et al. 2014; Neubauer et al., 2015). Here, after CH_4 fluxes were converted into CO_2-equivalent emission estimates assuming a 100 year CH_4 sustained-flux global warming potential [i.e., 1 kg CH_4=45 kg of CO_2; Neubauer et., al (2015)], CH_4 accounted for ~ 50% of CO_2-equivalent emissions from the estuary for both seasons, and therefore was significant in terms of greenhouse gas emissions.

4.3. Carbon surface water exports

Table 5 presents estimates of DIC and DOC export to coastal waters from small estuarine and large riverine systems. In a review paper, Cai (2011) reported the global riverine DOC export rate to be 246 Tg y^{-1}. Bauer and Bianchi (2011) also reported a similar global oceanic DOC export rate (250 Tg yr^{-1}). Based on the world wide surface areas of estuaries which is 1.05×10^{12} m^2 (Cai 2011), global DOC export from estuarine systems is estimated to be 0.64 g C m^{-2} d^{-1}. Hat Head estuary exported 15.5 g C m^{-2} of estuary d^{-1} of DOC, which is 24 times higher than the global estuarine DOC export estimate. DOC export from Hat Head estuary was also higher than much larger riverine systems (Striegl et al. 2007; Cai et al. 2008). Based on Table 5, DOC exports from systems of a similar small size to Hat Head estuary are higher, however, it

should be noted that exports reported in Adame and Lovelock (2011), Bergamaschi et al. (2012), Maher et al. (2013a), Wang and Cai (2004) and Winter et al. (1996) are from mangrove or salt marsh systems which essentially have a minimal catchment area to water area ratio, thereby inflating the mmol C m^{-2} catchment d^{-1} (i.e. essentially all the catchment is intertidal). Moreover, DIC exports from the small Hat Head estuary had much higher DIC exports than larger riverine systems on a catchment area basis (Table 5). Hat Head estuary DIC yield (i.e. export per unit of catchment area), were 4 times higher than the Gulf of Trieste catchment (Tamše et al. 2014), 11–40 times higher than the Yukon River (Striegl et al. 2007), 16 – 55 times higher than the 6 largest Arctic Rivers (Tank et al. 2012) and two orders of magnitude higher than DIC exports reported for the Chena River in Alaska (Cai et al. 2008) and the Guadalquivir Estuary, Spain (De La Paz et al. 2007). In comparison with smaller estuaries, Hat Head DIC yield was two orders of magnitude higher than the York River estuary (Raymond et al. 2000) and comparable with intertidal mangrove and saltmarsh systems (Wang and Cai 2004, Bouillon et al. 2008; Maher et al. 2013a; Winter et al. 1996).

The source of DIC is possibly from the surrounding mangroves, as Hat Heat estuary has an extensive mangrove environment throughout the estuary (Fig. 1). Mangrove environments tend to have high DIC export rates (Bouillon et al. 2008; Miyajima et al. 2009; Maher et al. 2013a). Moreover, a DIC vs. salinity scatter graph (Fig. 5) showed a slight concave upward trend (at least in the dry season) which suggests mid-estuary inputs of DIC (perhaps from mangrove groundwater). DOC, however, had a conservative or sink nature in relation to salinity (Fig. 5), which suggests an upstream source (likely the freshwater wetlands or groundwater, see also Sanders et al., 2015) with some loss during estuarine transport (respiration, photomineralization or flocculation). Our mass balance approach suggests significant groundwater inputs of all

475 dissolved carbon species, yet the traditional salinity mixing model approach does not indicate a
476 clear source. Wang et al. (2015) found a significant groundwater source of DIC in the Jiulong
477 estuary (China), yet salinity versus DIC indicated conservative mixing. The authors suggested
478 that the diffuse nature of SGD-derived solute inputs may lead to no deviation from conservative
479 mixing, which may also be the case in Hat Head estuary, and other estuarine systems that have
480 large areas of diffuse groundwater input along the estuary.

481 Alkalinity export to the coastal ocean ranged from 19 to 27 mmol m^{-2} of catchment d^{-1} in dry
482 and wet seasons, respectively (Table 4). Previous studies have reported alkalinity exports, from
483 larger systems, however, studies with time series sampling for calculating alkalinity exports from
484 tidal estuaries are still scarce. Faber et al. (2014) identified that DIC export was mostly alkalinity
485 in a mangrove and seagrass dominated tidal creek in southeast Australia. They reported export
486 rates ranging from 140–460 mmol m^{-2} of water area d^{-1}, which was an order of magnitude lower
487 than alkalinity export estimates from Hat Head estuary (3564 mmol m^{-2} of water area d^{-1}). Santos
488 et al. (2015) reported groundwater-derived alkalinity exports 4.7 times higher than Hat Head
489 from tidal flats in the Wadden Sea (Germany) where porewater alkalinity concentrations are
490 extremely high at 20 mM. Alkalinity production has a significant influence on the global carbon
491 budgets by affecting the oceanic carbonate system. In the case of alkalinity production, carbon is
492 not lost to the atmosphere as CO_2, and is exported to the ocean and acts as a buffer which
493 facilitates the uptake of extra CO_2 (Faber et al. 2014).

494 Table 5 shows that a general negative correlation may exist between dissolved carbon yield
495 and catchment area, and that small estuarine systems have the ability to deliver more dissolved
496 organic carbon to the coastal ocean compared to larger riverine systems on a catchment area
497 basis. This is mainly due to the shorter residence time of estuaries which reduces the potential for

biogeochemical processes to modify the quantity and composition of organic matter. This highlights the importance of studying small systems with a short residence time, such as Hat Head, to obtain a better quantitative understating of global carbon exports to the ocean.

4.4. Groundwater-derived carbon fluxes

We could not collect deep groundwater samples during the wet season, and shallow samples were only collected from the most downstream station during the wet season field campaign. We acknowledge the limitations with this approach. However, shallow samples collected at the downstream station were similar during both seasons (averages within 10%), and previous studies have found that deep groundwater has relatively stable composition (Dhar et al., 2008; Chapagain et al., 2010). Further, shallow groundwater only dominates inputs during the dry season (Sadat-Noori et al., 2015), when we have adequate sampling coverage throughout the estuary to constrain the shallow groundwater endmember. Considering the uncertainty in shallow groundwater composition during the wet season (i.e. we have used the dry season data to estimate this), we have assigned a 100% uncertainty to this term in our calculations (Table 4). The relative contributions of deep and shallow groundwater carbon inputs during wet and dry seasons basically follows the groundwater discharge rates with deep groundwater dominating carbon inputs in the wet season and shallow groundwater delivering more carbon in the dry season. Groundwater fluxes of each carbon species could not be calculated for each individual section during each season due to the lack of groundwater and surface water samples in the upper reaches of the estuary. Surface water samples were only collected at the downstream station for carbon parameters other than pCO_2.

520 Another limitation to our groundwater fluxes is that the average flux presented here only
521 considers the differences between the wet and dry season while other factors such as differences
522 in spring-neap tide cycles and annual temperature variability may influence the groundwater
523 discharge flux (de Sieyes et al., 2008; Constantz et al., 1994) and estuarine carbon fluxes.
524 Moreover, tidal variability can also influence groundwater discharge rates and consequently
525 carbon fluxes, as tidal pumping releases shallow saline groundwater into the estuary (Call et al.,
526 2015, Maher et al 2015, Santos et al., 2009). Tidal pumping was the dominant source of
527 groundwater discharge in the dry season making the shallow saline groundwater contribution
528 much higher than deep fresh groundwater. Therefore, some of the differences that were observed
529 may be due to differences in tidal pumping.

530 Most of the carbon input to surface waters via groundwater was in the form of DOC and
531 DIC and the smallest portion was contributed by CH_4 (1%) in both seasons (Fig. 6). The total
532 groundwater-derived DIC flux entering surface waters was 4.6 times higher in the wet season
533 compared to dry. While the total (deep + shallow) average groundwater-derived DIC fluxes from
534 both seasons (687 ± 117 mmol m^{-2} of estuary d^{-1}) were comparable to previous studies by Santos
535 et al. (2012a), Dorsett et al. (2011) and Cai (2003) (see Table 6), higher DIC fluxes have been
536 reported in salt marshes/estuaries (Moore et al. 2006) and fresh water tidal creeks (Atkins et al.
537 2013) (Table 6). The total (deep + shallow) average (wet and dry) groundwater-derived DOC
538 fluxes found here (540 ± 731 mmol m^{-2} d^{-1}) are high, being at least 3 fold higher than previous
539 studies which have reported groundwater-derived DOC fluxes ranging from 21 to 170 mmol m^{-2}
540 d^{-1} (Santos et al. 2012a; Maher et al. 2013a; Porubsky et al. 2014) (Table 6). These high fluxes
541 are related to the high DOC concentrations in groundwater (Table 1).

542 pCO_2 in the water column was positively correlated with radon (Fig. 5), indicating that
543 groundwater is a source of free CO_2 and/or $[H^+]$. The strong relationship between pCO_2, CH_4 and
544 radon (groundwater tracer) during both wet and dry season field campaigns (Fig. 5), in addition
545 to the high groundwater pCO_2 and CH_4 concentrations, implies groundwater was a major driver
546 of surface water pCO_2 and CH_4 in Hat Head estuary. This influence could either be directly by
547 discharging pCO_2 and CH_4 enriched groundwater into the estuary or indirectly by groundwater
548 delivering DOC, which can boost ecosystem respiration and increase pCO_2 (Maher et al. 2015).
549 The later process is further supported by the DOC vs. radon plot (Fig. 5) which shows a positive
550 correlation. The salinity mixing plots (Fig. 5) show that pCO_2 and CH_4 have a concave trend
551 with salinity indicating an upstream input likely being groundwater discharge from the upper
552 reaches as this area was found to be a groundwater hotspot in a concurrent study by Sadat-Noori
553 et al., (2015).

554 Flux calculations offer stronger evidence that groundwater plays a major role in delivering
555 greenhouse gasses to surface waters. The fluxes obtained from the groundwater mass balance
556 approach show that groundwater-derived free CO_2 and CH_4 inputs can account for a large
557 proportion (54% for CO_2 and 46% for CH_4) of the observed atmospheric fluxes (Table 3).
558 Previous studies have also found groundwater to be a major driver of surface water pCO_2 and
559 CH_4 (Faber et al. 2014; Macklin et al. 2014; Call et al. 2015). Atkins et al. (2013) reported that
560 groundwater-derived CO_2 fluxes into a flood plain creek estuary, NSW, Australia, averaged 1622
561 mmol m^{-2} d^{-1}, a value twice as high as atmospheric CO_2 evasion in the area, and 1.5 times larger
562 than CO_2 fluxes in our case. Conversely, Porubsky et al. (2014) stated groundwater-derived CH_4
563 fluxes were 0.8 mmol m^{-2} d^{-1} in Okatee estuary in USA, 15 times smaller than fluxes from Hat
564 Head estuary.

565 Radon also had a positive correlation with DOC especially in the wet season, but not as clear
566 as pCO_2 and CH_4, likely due to multiple processes driving surface water DOC dynamics in this
567 system. For example, radon and DOC may have the same source (groundwater) but have
568 different loss pathways as radon is a gas and its major loss source is atmospheric evasion, while
569 DOC maybe lost through respiration, flocculation and photomineralization. This creates a
570 decoupling between radon and DOC which may not be so apparent as in the radon vs CO_2 and
571 CH_4 plots (Fig. 5) and explains the stronger correlation between radon and the greenhouse gases.
572 Estuarine CO_2 is driven by biological (productivity/respiration), hydrological (groundwater
573 inputs and mixing of riverine and oceanic waters) and physical (temperature driven groundwater
574 convection and wind driven evasion) process (Borges and Abril 2011; Maher et al. 2015). Here,
575 the contribution of groundwater to CO_2 loss (evasion and export (Table 3 and 4)) from the
576 estuary was on average 31% over both seasons. The groundwater contribution to CH_4 loss
577 (evasion and export) was around 46%, with significant differences in wet and dry seasons. This
578 can be explained through the difference in the groundwater discharge rate between wet and dry
579 seasons (Table 2), where the groundwater contribution is a function of groundwater discharge
580 (which varied significantly in different hydrological conditions at our site) and groundwater end-
581 member concentration (which was assumed to be the same during both seasons).
582 Dissolved carbon is transported from groundwater to the estuary and then the atmosphere
583 (CO_2 and CH_4) and the ocean (DIC and DOC). Figure 3 illustrates this for CO_2, where oceanic
584 waters enter the estuary with the flood tide, becomes enriched in dissolved carbon within the
585 estuary due to mixing with groundwater (and upstream wetland surface water) and leaves the
586 system via ebb tide flow and atmospheric evasion. By investigating the CO_2 versus salinity plot
587 for the 4 stations (Fig. 7) we found hysteresis occurring at some stations with different CO_2

588 values at the same salinity during the ebb and flood tide. For instance, observations at station 3 in
589 the wet season showed that as the salinity starts to decrease from flood tide, CO_2 remains low for
590 8 hours. This continues until brackish waters occupy the station (salinity ~ 8), implying that the
591 initial fresh water entering the estuary is fresh surface water relatively low in CO_2. A subsequent
592 increase in CO_2 values imply the input of groundwater during the ebb tide, indicating a delayed
593 groundwater input to the estuary. This interpretation is supported by the CO_2 vs. radon scatter
594 that shows no hysteresis (Figure 5).

595 Total average groundwater-derived CH_4 fluxes (12 ± 17 mmol m^{-2} d^{-1}) (Table 2) were much
596 higher than groundwater-derived CH_4 fluxes from a small tidal river estuary, in Okatee, USA
597 (0.9 mmol m^{-2} d^{-1}, Porubsky et al. 2014). They were also three orders of magnitude higher than
598 CH_4 fluxes on the Florida Gulf Coast (Cable et al. 1996). Groundwater-derived CH_4 fluxes were
599 accountable for almost all the export from the estuary, and much of the free CO_2 export could be
600 attributed to groundwater inputs (Table 4) indicating the major role of groundwater in CH_4 and
601 dissolved CO_2 transported between terrestrial and aquatic environments.

602 Average DIC and DOC export from the estuary (3081 ± 602 and 1317 ± 258 mmol m^{-2} d^{-1},
603 respectively) were 4.4 and 2.4 fold higher than groundwater-derived DIC (687 ± 117 mmol m^{-2} d^{-1})
604 and DOC (540 ± 731 mmol m^{-2} d^{-1}) indicating that groundwater can account for almost half of
605 the dissolved organic carbon export from the estuary. In other words, the average contribution of
606 groundwater to DOC export in both seasons was ~ 41% while groundwater contributed ~ 22% to
607 DIC export with considerable differences in wet and dry seasons (Table 4). Maher et al. (2013a)
608 also found that groundwater advection was a dominant pathway for DOC export, and was
609 responsible for 90% of DOC export in a mangrove tidal estuary. Faber et al. (2014) reported that
610 90% of the carbon loss from an estuary system was from groundwater DIC advection while DOC

611 only accounted for 5%. Liu et al. (2014) reported that groundwater DIC fluxes were 11–71 times
612 higher than the combined input of local rivers, suggesting that SGD was the dominant source of
613 DIC to the southwest Florida Shelf, USA. Wang et al. (2015) found that SGD input of DIC to the
614 Jiulong River estuary in China was the equivalent to between 25% and 110% of riverine DIC
615 exports.

616 Groundwater had a minor contribution to TAlk input into the estuary (~ 3%) in both
617 seasons (Table 4). Average alkalinity export from estuary was almost 28 fold higher than
618 groundwater-derived alkalinity inputs, suggesting that processes other than groundwater input
619 are driving alkalinity export from this system. This alkalinity is thought to come from sulphate
620 reduction in shallow porewaters (Faber et al. 2014), however, our groundwater sampling
621 resolution was not adequate to capture this process (alkalinity may be produced in the upper cm
622 of sediments, while our groundwater samples were taken from areas deeper than 1 m).

623 To summarize the key findings of this study, we present a conceptual diagram (Fig. 8) that
624 illustrates the (1) groundwater discharge rates, (2) flux estimates of groundwater-derived carbon
625 into the estuary, (3) estuary carbon export and (4) carbon atmospheric evasion in wet and dry
626 conditions in the whole estuary system. The large variability observed in groundwater discharge
627 and carbon loss rates over a relatively short time scale indicates the need for more frequent
628 measurements to be carried to assess the influence of groundwater on carbon cycling.
629 Nevertheless, it is clear that this small wetland-surrounded subtropical estuary has a high carbon
630 yield (in terms of both oceanic export and air-water exchange), and groundwater carbon inputs
631 play a major role in estuarine carbon cycling in this system. Combined with the recent literature,
632 this investigation demonstrates that groundwater may play a major role in estuarine carbon
633 dynamics.

5. Conclusions

The Hat Head estuary, had a high area normalised export rate of DIC (3081 ± 602 mmol m^{-2} d^{-1}), DOC (1317 ± 258 mmol m^{-2} d^{-1}) and TAlk (3564 ± 705 mmol m^{-2} d^{-1}) to the coastal ocean and groundwater-derived carbon inputs were a significant component of this carbon export. Groundwater contribution to carbon loss from the estuary for DIC, DOC, TAlk, free CO_2 and CH_4 was found to be approximately 22%, 41%, 3%, 75% and 100%, respectively. The average estuary-wide CO_2 and CH_4 evasion rates were 870 ± 174 and 26 ± 5 mmol m^{-2} d^{-1} (some of the highest estuarine fluxes reported yet), and groundwater discharge accounted for 54% and 46% of these evasions, respectively. Our observations indicate that small estuarine systems with a short residence time can pump more carbon to the coastal ocean compared to some larger riverine systems on a catchment area basis, and that groundwater exchange may deliver large amounts of carbon to surface estuarine waters.

Acknowledgements

We would like to thank Christian Sanders, Luciana Sanders, Paul Macklin, Ashley McMahon, Benjamin Stewart, Jennifer Taylor and Judith Rosentreter for their support during field campaigns. IRS and DTM are funded through Australian Research Council DECRA Fellowships (DE140101733, and DE150100581). We acknowledge support from the Australian Research Council (DP120101645, LE120100156). We would also like to acknowledge the Associate Editor Alberto Borges and 2 anonymous reviewers for their constructive comments which helped strengthen our manuscript.

References

Abril, G., and N. Iversen. 2002. Methane dynamics in a shallow non-tidal estuary (Randers Fjord, Denmark). Mar. Ecol.: Prog. Ser. **230:** 171-181.

Abril, G., Bouillon, S., Darchambeau, F., Teodoru, C.R., Marwick, T.R., Tamooh, F., Ochieng Omengo, F., Geeraert, N., Deirmendjian, L., Polsenaere, P. and Borges, A.V., 2015. Technical Note: Large overestimation of pCO_2 calculated from pH and alkalinity in acidic, organic-rich freshwaters. Biogeosciences, 12(1): 67-78.

Adame, M. F., and C. E. Lovelock. 2011. Carbon and nutrient exchange of mangrove forests with the coastal ocean. Hydrobiologia, **663:** 23-50.

Atkins, M. L., I. R. Santos, S. Ruiz-Halpern, and D. T. Maher. 2013. Carbon dioxide dynamics driven by groundwater discharge in a coastal floodplain creek. J. Hydrol., **493:** 30-42.

Bauer, J., and T. Bianchi. 2011. Dissolved organic carbon cycling and transformation. Treatise on Estuarine and Coastal Science, **5:** 7-67.

Bergamaschi, B. A., D. P. Krabbenhoft, G. R. Aiken, E. Patino, D. G. Rumbold, and W. H. Orem. 2012. Tidally driven export of dissolved organic carbon, total mercury, and methylmercury from a mangrove-dominated estuary. Environ. Sci. Technol., **46:** 1371-1378.

Bianchi, T. S. 2007. Biogeochemistry of estuaries. Oxford University Press New York.

Borges, A. V., and Abril, G. 2011. Carbon dioxide and methane dynamics in estuaries. In E. Wolanski & D. S. McLusky (Eds.), Treatise on estuarine and coastal science. (Vol. 5, pp. 119-161). Waltham: Academic Press.

Borges, A., B. Delille, L.-S. Schiettecatte, F. Gazeau, G. Abril, and M. Frankignoulle. 2004. Gas transfer velocities of CO_2 in three European estuaries (Randers Fjord, Scheldt and Thames). Limnol. Oceanogr., **49:** 1630-1641.

Bouillon, S. and others 2007. Importance of intertidal sediment processes and porewater exchange on the water column biogeochemistry in a pristine mangrove creek (Ras Dege, Tanzania). Biogeosciences Discussions, **4:** 317-348.

Bouillon, S. and others 2008. Mangrove production and carbon sinks: a revision of global budget estimates. Global Biogeochem. Cycles, **22**. DOI: 10.1029/2007GB003052

Burnett, W. C. and others 2006. Quantifying Submarine Groundwater Discharge in the Coastal Zone via Multiple Methods. Sci. Total Environ., **367:** 498-543.

Burnett, W. C., R. N. Peterson, I. R. Santos, and R. W. Hicks. 2010. Use of automated radon measurements for rapid assessment of groundwater flow into Florida streams. J. Hydrol., **380:** 298-304.

Cable, J. E., G. C. Bugna, W. C. Burnett, and J. P. Chanton. 1996. Application of ^{222}Rn and CH_4 for assessment of groundwater discharge to the coastal ocean. Limnol. Oceanogr., **41:** 1347-1353.

Cai, W. J. 2003. The geochemistry of dissolved inorganic carbon in a surficial groundwater aquifer in North Inlet, South Carolina, and the carbon fluxes to the coastal ocean Geochimica et Cosmochimica Acta., **67:** 631– 637.

Cai, W.-J. 2011. Estuarine and Coastal Ocean Carbon Paradox: CO_2 Sinks or Sites of Terrestrial Carbon Incineration? Ann. Rev. Mar. Sci., **3:** 123-145.

Cai, Y., L. Guo, and T. A. Douglas. 2008. Temporal variations in organic carbon species and fluxes from the Chena River, Alaska. Limnol. Oceanogr., **53:** 1408-1419.

Call, M. and others 2015. Spatial and temporal variability of carbon dioxide and methane fluxes over semi-diurnal and spring-neap-spring timescales in a mangrove creek. Geochim. Cosmochim. Acta., **150**: 211-225.

Chapagain, S., K., V. P. Pandey, S. Shrestha, T. Nakamura, and F. Kazama. 2010. Assessment of Deep Groundwater Quality in Kathmandu Valley Using Multivariate Statistical Techniques. Water Air Soil Pollut., **210:**277-288.

Charette, M. A., and M. C. Allen. 2006. Precision Ground Water Sampling in Coastal Aquifers Using a Direct-Push, Shielded-Screen Well-Point System. Groundwater Monit. Rem., **26:** 87-93.

Chen, C.-T. A., T.-H. Huang, Y.-C. Chen, Y. Bai, X. He, and Y. Kang. 2012. Air–sea exchanges of CO_2 in the world's coastal seas. Biogeosciences, **10:** 6509-6544.

Constantz, J., C. L. Thomas, and G. Zellweger. 1994. Influence of diurnal variations in stream temperature on streamflow loss and groundwater recharge. Water Resour. Res., **30:** 3253-3264.

Cyronak, T., I. R. Santos, D. V. Erler, D. T. Maher, and B. D. Eyre. 2014. Drivers of pCO_2 variability in two contrasting coral reef lagoons: The influence of submarine groundwater discharge. Global Biogeochem. Cycles., **28**:398-414.

De La Paz, M., A. Gómez-Parra, and J. Forja. 2007. Inorganic carbon dynamic and air–water CO_2 exchange in the Guadalquivir Estuary (SW Iberian Peninsula). J. Mar. Sys., **68:** 265-277.

de Sieyes, N. R., K. M. Yamahara, B. A. Layton, E. H. Joyce, and A. B. Boehm. 2008. Submarine discharge of nutrient-enriched fresh groundwater at Stinson Beach, California is enhanced during neap tides. Limnol. Oceanogr., **53:**1434-1445.

Dhar, R.K., Y. Zhenga, A. van Geen, Z. Cheng, M. Shanewaz, M. Shamsudduha, M.A. Hoque, M.W. Rahman, K.M. Ahmed. 2008. Temporal variability of groundwater chemistry in shallow and deep aquifers of Araihazar, Bangladesh. J. Contam. Hydrol., **99:** 97–111

Dickson, A. G. 1990. Standard potential of the reaction: AgCl (s)+ 12H2 (g)= Ag (s)+ HCl (aq), and and the standard acidity constant of the ion HSO_4^- in synthetic sea water from 273.15 to 318.15 K. J. Chem.Thermodyn., **22:** 113-127.

Dixon, J. L., J. R. Helms, R. J. Kieber, and G. B. Avery. 2014. Biogeochemical alteration of dissolved organic material in the Cape Fear River Estuary as a function of freshwater discharge. Estuar. Coast. Shelf Sci., **149:** 273-282.

Dorsett, A., Jennifer Cherrier A, J. B. Martin, and J. E. Cable. 2011. Assessing hydrologic and biogeochemical controls on pore-water dissolved inorganic carbon cycling in a subterranean estuary: A 14C and 13C mass balance approach. Mar. Chem., **127:** 76-89.

Faber, P. A., V. Evrard, R. J. Woodland, I. C. Cartwright, and P. L. Cook. 2014. Pore-water exchange driven by tidal pumping causes alkalinity export in two intertidal inlets. Limnol. Oceanogr., **59:** 1749-1763.

Ferrón, S., T. Ortega, A. Gómez-Parra, and J. Forja. 2007. Seasonal study of dissolved CH_4, $CO_2$and N_2O in a shallow tidal system of the bay of Cádiz (SW Spain). Journal of Marine Systems, **66:** 244-257.

Frankignoulle, M. and others 1998. Carbon dioxide emission from European estuaries. Science, **282:** 434-436.

Frankignoulle, M., I., Bourge, and R. Wollast,1996. Atmospheric CO_2 fluxes in a highly polluted estuary (the Scheldt). Limnol. Oceanogr., **41:** 365-369.

Gagan, M. K., L. K. Ayliffe, B. N. Opdyke, D. Hopley, H. Scott-Gagan, and J. Cowley. 2002. Coral oxygen isotope evidence for recent groundwater fluxes to the Australian Great Barrier Reef. Geophys. Res. Lett., **29:** 43-1 - 43-4.

Gatland, J. R., I. R. Santos, D. T. Maher, T. Duncan, and D. V. Erler. 2014. Carbon dioxide and methane emissions from an artificially drained coastal wetland during a flood: Implications for wetland global warming potential. Geophys. Res. Res.: Biogeosciences **119:** 1698-1716.

Gazeau, F. and others 2005. Planktonic and whole system metabolism in a nutrient-rich estuary (the Scheldt estuary). Estuaries Coasts, **28:** 868-883.

748 Gleeson, J., I. R. Santos, D. T. Maher, and L. Golsby-Smith. 2013. Groundwater–surface water exchange
749 in a mangrove tidal creek: Evidence from natural geochemical tracers and implications for
750 nutrient budgets. Mar. Chem., **156**: 27-37.
751 Goñi, M. A., and I. R. Gardner. 2003. Seasonal dynamics in dissolved organic carbon concentrations in a
752 coastal water-table aquifer at the forest-marsh interface. Aquat. Geochem., **9:** 209-232.
753 Hans, H. D., G. Laruelle, G., C. M. Van Kempen, C. P. Slomp, M. Meybeck, and H. Middelkoop. 2011.
754 Worldwide Typology of Nearshore Coastal Systems: Defining the Estuarine Filter of River Inputs
755 to the Oceans. Estuaries Coasts, **34:** 441–458.
756 Hunt, C.W., Salisbury, J.E. and Vandermark, D., 2011. Contribution of non-carbonate anions to total
757 alkalinity and overestimation of pCO_2 in New England and New Brunswick rivers. Biogeosciences,
758 **8:** 3069-3076.
759 Kim, G., J.-S. Kim, and D.-W. Hwang. 2011. Submarine groundwater discharge from oceanic islands
760 standing in oligotrophic oceans: Implications for global biological production and organic carbon
761 fluxes. Limnol. Oceanogr., **56:** 673-682.
762 Lee, J.-M., and G. Kim. 2006. A simple and rapid method for analyzing radon in coastal and ground
763 waters using a radon-in-air monitor. J. Environ. Radioact., **89:** 219-228.
764 Linto, N., J. Barnes, R. Ramachandran, J. Divia, P. Ramachandran, and R. Upstill-Goddard. 2014. Carbon
765 dioxide and methane emissions from mangrove-associated waters of the Andaman Islands, Bay
766 of Bengal. Estuaries Coasts, **37:** 381-398.
767 Liu, Q. and others 2012. How significant is submarine groundwater discharge and its associated
768 dissolved inorganic carbon in a river-dominated shelf system? Biogeosciences, **9:** 1777-1795.
769 Liu, Q., M. A. Charette, P. B. Henderson, D. C. Mccorkle, W. Martin, and M. Dai. 2014. Effect of
770 submarine groundwater discharge on the coastal ocean inorganic carbon cycle. Limnol.
771 Oceanogr., **59:** 1529-1554.
772 Macklin, P. A., D. T. Maher, and I. R. Santos. 2014. Estuarine canal estate waters: Hotspots of CO_2
773 outgassing driven by enhanced groundwater discharge? Mar. Chem., **167:** 82-92.
774 Maher, D and B. D. Eyre 2012. Carbon budgets for three autotrophic Australian estuaries: Implications
775 for global estimates of the coastal air-water CO_2 flux. Global Biogeochem. Cycles, **26**. DOI:
776 10.1029/2011GB004075.
777 Maher, D. T. and others 2013b. Novel use of cavity ring-down spectroscopy to investigate aquatic
778 carbon cycling from microbial to ecosystem scales. Environ. Sci. Technol., **47:** 12938-12945.
779 Maher, D. T., and B. D. Eyre. 2010. Benthic fluxes of dissolved organic carbon in three temperate
780 Australian estuaries: Implications for global estimates of benthic DOC fluxes. J. Geophys. Res.:
781 Biogeosci. (2005–2012) **115**, G04039, doi:10.1029/2010JG001433.
782 Maher, D. T., I. R. Santos, L. Golsby-Smith, J. Gleeson, and B. D. Eyre. 2013a. Groundwater-derived
783 dissolved inorganic and organic carbon exports from a mangrove tidal creek: The missing
784 mangrove carbon sink? Limnol. Oceanogr., **58:** 475-488.
785 Maher, D. T., K. Cowley, I. R. Santos, P. Macklin, and B. D. Eyre. 2015. Methane and carbon dioxide
786 dynamics in a subtropical estuary over a diel cycle: Insights from automated in situ radioactive
787 and stable isotope measurements. Mar. Chem., **168:** 69-79.
788 Maher, D., and B. D. Eyre. 2011. Insights into estuarine benthic dissolved organic carbon (DOC) dynamics
789 using δ13C-DOC values, phospholipid fatty acids and dissolved organic nutrient fluxes. Geochim.
790 Cosmochim. Acta, **75:** 1889-1902.
791 Millero, F. J., T. B. Graham, F. Huang, H. Bustos-Serrano, and D. Pierrot. 2006. Dissociation constants of
792 carbonic acid in seawater as a function of salinity and temperature. Mar. Chem., **100:** 80-94.
793 Miyajima, T., Y. Tsuboi, Y. Tanaka, and I. Koike. 2009. Export of inorganic carbon from two Southeast
794 Asian mangrove forests to adjacent estuaries as estimated by the stable isotope composition of

dissolved inorganic carbon. J. Geophys. Res.: Biogeosci. (2005–2012) **114**, DOI: 10.1029/2008JG000861.

Moore, W. S. 2010. The effect of submarine groundwater discharge on the ocean. Ann. Rev. Mar. Sci., **2:** 59-88.

Moore, W. S., and R. Arnold. 1996. Measurement of ^{223}Ra and ^{224}Ra in coastal waters using a delayed coincidence counter. J. Geophys. Res.: Oceans (1978–2012) **101:** 1321-1329.

Moore, W. S., J. O. Blanton, and S. B. Joye. 2006. Estimates of flushing times, submarine groundwater discharge, and nutrient fluxes to Okatee Estuary, South Carolina. J. Geophys. Res.: Oceans (1978–2012) **111**, DOI: 10.1029/2005JC003041.

Neubauer, S. C., and J. P., Megonigal, 2015. Moving beyond global warming potentials to quantify the climatic role of ecosystems. Ecosystems, **18**(6): 1000-1013.

Nirmal Rajkumar, A., J. Barnes, R. Ramesh, R. Purvaja, and R. Upstill-Goddard. 2008. Methane and nitrous oxide fluxes in the polluted Adyar River and estuary, SE India. Mar. Pollut. Bull., **56:** 2043-2051.

Noriega, C., and M. Araujo. 2014. Carbon dioxide emissions from estuaries of northern and northeastern Brazil. Scientific reports, **4**, 6164.

O'Reilly, C., I.R. Santos, T. Cyronak, A. McMahon and D.T. Maher. 2015. Nitrous oxide and methane dynamics in a coral reef lagoon driven by porewater exchange: Insights from automated high frequency observations. Geophys. Res. Lett. **42**(8), DOI: 10.1002/2015GL063126.

Panneer Selvam, B., S. Natchimuthu, L. Arunachalam, and D. Bastviken. 2014. Methane and carbon dioxide emissions from inland waters in India–implications for large scale greenhouse gas balances. Global change biol., **20**: 3397-3407.

Pelletier, G., Lewis, E., and Wallace, D. 2007. CO_2Sys. xls: A calculator for the CO_2 system in seawater for microsoft excel/VBA. Washington State Department of Ecology/Brookhaven National Laboratory, Olympia, WA/Upton, NY, USA.

Peterson, R. N., W. C. Burnett, N. Dimova, and I. R. Santos. 2009. Comparison of measurement methods for radium-226 on manganese-fiber. Limnol. Oceanogr.: Methods, **7:** 196–205.

Porubsky, W. P., N. B. Weston, W. S. Mooreb, C. Ruppel, and S. B. Joye. 2014. Dynamics of submarine groundwater discharge and associated fluxes of dissolved nutrients, carbon, and trace gases to the coastal zone (Okatee River estuary, South Carolina). Geochim. Cosmochim. Acta, **131** 81–97.

Raymond, P. A., J. E. Bauer, and J. J. Cole. 2000. Atmospheric CO_2 evasion, dissolved inorganic carbon production, and net heterotrophy in the York River estuary. Limnol. Oceanogr., **45:** 1707-1717.

Rodríguez-Murillo, J., J. Zobrist, and M. Filella. 2015. Temporal trends in organic carbon content in the main Swiss rivers, 1974–2010. Sci. Total Environ., **502:** 206-217.

Ruprecht, J. E., and W. A. Timms. 2010. Hat Head Effluent Disposal Scheme – Ongoing Monitoring Results to September 2010. WRL Technical Report.

Sadat-Noori, M., Santos, I., Maher, D., Sanders, C. and Sanders, L., 2015. Groundwater Discharge into an Estuary Using Spatially Distributed Radon Time Series and Radium Isotopes. J. Hydrol., **528:** 703-719.

Sanders, C. J., Santos, I. R., Maher, D. T., Sadat-Noori, M., Schnetger, B., and Brumsack, H.-J. (2015). Dissolved iron exports from an estuary surrounded by coastal wetlands: Can small estuaries be a significant source of Fe to the ocean? Mar. Chem., **176:** 75-82.

Santos I. R., W. C. Burnett, T. Dittmar, I. G.N.A. Suryaputra, and J. Chanton. 2009. Tidal pumping drives nutrient and dissolved organic matter dynamics in a Gulf of Mexico subterranean estuary. Geochim. Cosmochim. Acta., **73**: 1325–1339.

Santos, I. R. and others 2015. Porewater exchange as a driver of carbon dynamics across a terrestrial-marine transect: Insights from coupled ^{222}Rn and pCO_2 observations in the German Wadden Sea. Mar. Chem., **171:** 10-20.

Santos, I. R., D. T. Maher, and B. D. Eyre. 2012b. Coupling automated radon and carbon dioxide measurements in coastal waters. Environ. Sci. Technol., **46:** 7685-7691.

Santos, I. R., P. L. M. Cook, L. Rogers, J. De Weys, and B. D. Eyre. 2012a. The ''salt wedge pump'': Convection-driven pore-water exchange as a source of dissolved organic and inorganic carbon and nitrogen to an estuary. Limnol. Oceanogr., **57:** 1415–1426.

Seitzinger, S., J. Harrison, E. Dumont, A. H. Beusen, and A. Bouwman. 2005. Sources and delivery of carbon, nitrogen, and phosphorus to the coastal zone: An overview of Global Nutrient Export from Watersheds (NEWS) models and their application. Global Biogeochem. Cycles, **19**, DOI: 10.1029/2005GB002606.

Stewart, B. T., I. R. Santos, D. R. Tait, P. A. Macklin, D. T. Maher. 2015. Submarine groundwater discharge and associated fluxes of alkalinity and dissolved carbon into Moreton Bay (Australia) estimated via radium isotopes. Mar. Chem., **174:** 20 1‑12.

St-Jean, G. 2003. Automated quantitative and isotopic (^{13}C) analysis of dissolved inorganic carbon and dissolved organic carbon in continuous-flow using a total organic carbon analyser. Rapid Commun. Mass Spectrom., **17:** 419-428.

Striegl, R. G., M. M. Dornblaser, G. R. Aiken, K. P. Wickland, and P. A. Raymond. 2007. Carbon export and cycling by the Yukon, Tanana, and Porcupine rivers, Alaska, 2001–2005. Water Resour. Res. **43**, DOI: 10.1029/2006WR005201.

Tamše, S., N. Ogrinc, L. M. Walter, D. Turk, and J. Faganeli. 2014. River Sources of Dissolved Inorganic Carbon in the Gulf of Trieste (N Adriatic): Stable Carbon Isotope Evidence. Estuaries Coasts**, 38(1):** 1-14.

Tank, S. E. and others 2012. A land-to-ocean perspective on the magnitude, source and implication of DIC flux from major Arctic rivers to the Arctic Ocean. Global Biogeochem. Cycles, **26**. DOI: 10.1029/2011GB004192.

Wang, G. and others 2015. Net subterranean estuarine export fluxes of dissolved inorganic C, N, P, Si, and total alkalinity into the Jiulong River estuary, China. Geochim. Cosmochim. Acta. **149**: 103-114.

Wang, Z. A., and W.-J. Cai. 2004. Carbon dioxide degassing and inorganic carbon export from a marsh-dominated estuary (the Duplin River): A marsh CO_2 pump. Limnol. Oceanogr., **49:** 341-354.

Wanninkhof, R. 1992. Relationship between wind speed and gas exchange over the ocean. J. Geophys. Res.: Oceans (1978–2012) **97:** 7373-7382.

Weinstein, Y., W. Burnett, P. Swarzenski, Y. Shalem, Y. Yechieli, and B. Herut. 2007. Role of aquifer heterogeneity in fresh groundwater discharge and seawater recycling: An example from the Carmel coast, Israel. J. Geophys. Res. :Oceans (1978–2012) **112**, DOI: 10.1029/2007JC004112.

Weiss, R. F. 1974. Carbon dioxide in water and seawater: the solubility of a non-ideal gas. Mar. Chem., **2:** 203-215.

Wiesenburg, D. a., and N. L. Guinasso. 1979. Equilibrium solubilities of methane, carbon monoxide, and hydrogen in water and sea water. J. Chem. Eng. Data, **24**(4)**:** 356-360.

Winter, P. E., T. A. Schlacherl, and D. Baird. 1996. Carbon flux between an estuary and the ocean: a case for outwelling. Hydrobiologia, **337:** 123-132.

Zhang, G., J. Zhang, S. Liu, J. Ren, J. Xu, and F. Zhang. 2008. Methane in the Changjiang (Yangtze River) Estuary and its adjacent marine area: riverine input, sediment release and atmospheric fluxes. Biogeochemistry, **91:** 71-84.

888 **Figure legends**
889
890 Figure 1. Study site (Had Head, NSW, Australia) displaying the time series stations (green points) and
891 groundwater sampling locations (red points). The distance between stations 1 - 2 and 2 - 3 is 1.5 km,
892 while stations 3 - 4 are 1 km apart. The dark box represents the study site. The entire estuary length was
893 fringed by mangroves. All carbon species were measured in Station 1, while only pCO_2 data are available
894 for Stations 2-4. Image from Google Earth.
895
896 Figure 2. Surface water time series data from the downstream station located at the mouth of the estuary
897 in the wet (March) and dry (June) seasons. The radon data are reported in our companion paper Sadat-
898 Noori et al. (2015).
899
900 Figure 3. Time series of partial pressure of CO_2 from the four stations in the wet season, and two stations
901 in the dry season.
902
903 Figure 4. Calculated versus measured DIC in surface water and groundwater from the downstream station
904 located at the mouth of the estuary in wet and dry seasons. The line represents the 1:1 ratio.
905
906 Figure 5. DIC, DOC, Alkalinity, pCO_2 and CH_4 vs. radon, salinity and depth in estuary surface water in
907 wet (March) and dry (June) seasons from the downstream station located at the mouth of the estuary.
908 Lines indicate the theoretical conservative mixing.
909
910 Figure 6. Average (wet and dry season) portions of carbon species derived by groundwater and losses
911 from the mouth of the estuary assuming that alkalinity fluxes are related to carbonate alkalinity.
912
913 Figure 7. CO_2 versus salinity scatter plots in wet and dry seasons at the four stations along the estuary
914 showing hysteresis.

915

916 Figure 8. Conceptual diagram of the study area summarizing flux estimates ± standard error of
917 groundwater-derived, estuary export and atmospheric evasion of carbon from the mouth of the estuary in
918 (a) wet and (b) dry seasons. Groundwater discharge rates are in m^{-3} s^{-1} and all other parameters are in
919 units of 10^4 mols d^{-1} (estuary area = 116,160 m^2 and catchment area = 18 km^2).

920

921 **Table 1.** Groundwater observations.

Sample ID	Date	Longitude	Latitude	Depth (m)	Salinity	pH	^{222}Rn (Bq m^{-3})	Alkalinity (µM)	DIC (µM)	DOC (µM)	Free CO_2 (µM)	CH_4 (µM)
						Shallow						
GW 1	7/06/2013	S31.057	E153.056	1.5	30.9	8.5	25	2707	2055	271	3	0.02
GW 2	7/06/2013	S31.057	E153.056	1.5	25.7	8.5	1599	2617	2101	182	4	0.2
GW 3	8/06/2013	S31.057	E153.056	1.8	17.9	8.2	941	2057	1880	564	11	1
GW 4	12/06/2013	S31.0002	E153.0324	4	0.1	5.0	365	188	3345	5936	3146	152
GW 5	8/06/2013	S31.0071	E153.032	4	0.1	4.9	105	15	1333	6510	1295	14
GW 6	9/06/2013	S31.305	E153.038	2.5	0.2	4.6	27	22	1531	7728	1486	112
GW 7	9/06/2013	S31.056	E153.033	2	0.1	4.6	266	72	1455	4968	1372	31
GW 8	10/06/2013	S31.042	E153.034	2	2.2	6.6	605	1054	1404	2844	350	3
GW 9	10/06/2013	S31.042	E153.042	1.5	1.5	5.3	834	316	2254	1442	1934	5
GW 10	10/06/2013	S31.042	E153.042	2	0.1	4.9	250	24	672	776	636	0.1
GW 11	10/06/2013	S31.050	E153.042	1.5	14.8	5.8	470	960	2296	545	1335	10
GW 12	10/06/2013	S31.050	E153.050	1.2	0.3	6.7	587	1211	1488	2089	278	13
GW 13	10/06/2013	S31.050	E153.042	1.5	1.8	5.9	444	439	1157	1144	716	0.3
GW 14	11/06/2013	S31.069	E153.032	4.5	0.1	5.2	159	133	1386	533	1246	42
Median						5.6	405	378	1509	1293	981	8
ST Error						0.4	115	260	173	700	237	12
						Deep						
GW 15	12/06/2013	S30.997	E153.025	5.5	0.1	4.4	574	5	2159	7710	2118	116
GW 16	12/06/2013	S30.999	E153.027	16	0.1	5.2	1403	240	2204	1068	1958	172
GW 17	8/06/2013	S31.029	E153.026	10	0.2	4.7	209	9	931	6194	901	0.1
GW 18	8/06/2013	S31.007	E153.026	18	0.1	6.2	247	843	1569	370	725	54
GW 19	8/06/2013	S31.021	E153.024	6	0.1	6.0	135	845	2196	10230	1350	0.1
GW 20	8/06/2013	S31.021	E153.024	21	0.1	5.8	868	485	1402	320	929	177
GW 21	8/06/2013	S31.056	E153.036	11.7	0.2	4.7	181	26	1195	4985	1150	27
GW 22	9/06/2013	S31.053	E153.037	7.5	0.1	6.8	561	662	823	420	162	12
GW 23	11/06/2013	S31.068	E153.033	20	0.1	5.3	240	145	1190	51	1040	281
GW 24	11/06/2013	S31.068	E153.033	10.8	0.1	6.5	451	881	1293	950	412	53
GW 25	11/06/2013	S31.091	E153.013	10.5	0.1	5.5	103	271	1496	161	1222	84
GW 26	11/06/2013	S31.008	E153.025	11.7	0.1	5.3	501	152	1330	1330	995	42
GW 27	12/06/2013	S31.020	E153.024	5.5	0.1	4.8	416	35	1049	6704	999	30
Median						5.3	416	240	1330	1068	999	53
ST Error						0.2	100	96	130	982	148	23
							Total					
Median						5.4	416	271	1455	1144	999	27
ST Error						0.1	75	148	111	587	140	14

922

Table 2. Groundwater-derived carbon species into the estuary in units of mmol m^{-2} of estuary d^{-1}. SGD rates reported in Sadat-Noori et al. (2015) were used.

		Wet	Dry
Shallow			
SGD	(m^3 s^{-1})	0.33±0.09	0.19±0.23
DIC	(mmol m^{-2} d^{-1})	376±376	213±129
DOC	(mmol m^{-2} d^{-1})	322±322	183±521
Alkalinity	(mmol m^{-2} d^{-1})	94±94	53±193
Free CO_2	(mmol m^{-2} d^{-1})	244±244	138±177
CH_4	(mmol m^{-2} d^{-1})	2±2	1±9
Deep			
SGD	(m^3 s^{-1})	0.71±0.25	0.03±0.01
DIC	(mmol m^{-2} d^{-1})	702±97	34±97
DOC	(mmol m^{-2} d^{-1})	564±730	29±730
Alkalinity	(mmol m^{-2} d^{-1})	127±71	6±71
Free CO_2	(mmol m^{-2} d^{-1})	527±110	26±110
CH_4	(mmol m^{-2} d^{-1})	28±17	1±17
Total			
SGD	(m^3 s^{-1})	1.04±0.13	0.22±0.13
DIC	(mmol m^{-2} d^{-1})	1131±83	243±83
DOC	(mmol m^{-2} d^{-1})	889±436	191±587
Alkalinity	(mmol m^{-2} d^{-1})	211±110	45±148
Free CO_2	(mmol m^{-2} d^{-1})	777±104	167±139
CH_4	(mmol m^{-2} d^{-1})	20±10	4±14

Estuary area: 116,160 m^2
Catchment area: 18,000,000 m^2

928

929 **Table 3.** Average gas transfer velocity used in calculations (Equation 2), CO_2 and CH_4 evasion from the estuary
930 (Equation 1) and groundwater-derived CO_2 evasion (Equation 3) in areal units of mmol m^{-2} of estuary d^{-1} and
931 estuary wide units of mmol d^{-1}.

Season	Average gas transfer velocity	CO_2 atmospheric fluxes		GW-derived CO_2	CH_4 atmospheric fluxes		GW-derived CH_4
	m d^{-1}	mmol d^{-1}	mmol m^{-2} d^{-1}	mmol m^{-2} d^{-1}	mmol d^{-1}	mmol m^{-2} d^{-1}	mmol m^{-2} d^{-1}
Wet - (March)	3.0	13.1×10^{7}	1127.7	777	0.2×10^{7}	17.2	20
Dry - (June)	2.3	7.2×10^{7}	619.8	167	0.5×10^{7}	43.0	4
Average	2.7	10.1×10^{7}	869.4	472	0.3×10^{7}	25.8	12

932
933

Table 4. Carbon export from the estuary in units of mmol d^{-1} and carbon yield in mmol m^{-2} of catchment d^{-1}.

	Wet season				Dry season				Average		
	mmol d^{-1}	mmol m^{-2} d^{-1}	Shallow GW contribution (mmol d^{-1})	Deep GW contribution (mmol d^{-1})	mmol d^{-1}	mmol m^{-2} d^{-1}	Shallow GW contribution (mmol d^{-1})	Deep GW contribution (mmol d^{-1})	mmol d^{-1}	mmol m^{-2} d^{-1}	Total GW (Shallow + deep) (mmol d^{-1})
DIC	43.5×10^7 $\pm8.6\times10^7$ (48×10^7)*	24.1±4.7 (26) *	$43.6\times10^6\pm43.6\times10^6$	$81.5\times10^6\pm11.2\times10^6$	28.2×10^7 $\pm5.6\times10^7$ (29×10^7)*	15.6±3.1 (16) *	$24.7\times10^6\pm14.9\times10^6$	$4.0\times10^6\pm1.1\times10^6$	35.8×10^7 $\pm7.0\times10^7$	19.8±3.8	$77.0\times10^6\pm31.9\times10^6$
DOC	25.5×10^7 $\pm5.0\times10^7$	14.1±2.7	$37.4\times10^6\pm37.4\times10^6$	$65.5\times10^6\pm84.8\times10^6$	5.1×10^7 $\pm1.0\times10^7$	2.8±0.5	$2.1\times10^6\pm60.5\times10^6$	$3.2\times10^6\pm8.4\times10^6$	15.3×10^7 $\pm3.0\times10^7$	8.5±1.6	$63.7\times10^6\pm98.4\times10^6$
Alkalinity	48.7×10^7 $\pm9.6\times10^7$	27.0±5.3	$10.9\times10^6\pm10.9\times10^6$	$70.5\times10^6\pm82.5\times10^6$	34.2×10^7 $\pm6.8\times10^7$	19.0±3.7	$6.1\times10^6\pm22.4\times10^6$	$0.7\times10^6\pm8.2\times10^6$	41.4×10^7 $\pm8.2\times10^7$	23.0±4.5	$16.3\times10^6\pm18.8\times10^6$
Free CO_2	13.8×10^7 $\pm2.6\times10^7$	7.6±1.4	$28.4\times10^6\pm28.4\times10^6$	$61.3\times10^6\pm12.8\times10^6$	0.9×10^7 $\pm1.8\times10^6$	0.5±0.1	$16.1\times10^6\pm20.5\times10^6$	$19.8\times10^6\pm83.4\times10^6$	7.3×10^7 $\pm1.4\times10^7$	4.0±0.7	$35.1\times10^6\pm58.8\times10^6$
CH_4	0.009×10^7 $\pm0.0018\times10^7$	0.005 ±0.001	$2.2\times10^5\pm2.2\times10^5$	$3.2\times10^6\pm2.0\times10^6$	0.02×10^7 $\pm4.0\times10^4$	0.01 ±0.01	$0.1\times10^6\pm1.0\times10^6$	$0.2\times10^6\pm1.0\times10^6$	0.01×10^7 $\pm0.002\times10^7$	0.005 ±0.001	$0.5\times10^6\pm2.1\times10^6$

*Values in bracket indicate calculated DIC using TA and pCO_2.

Estuary area: 116160 m^2

Catchment area: 18,000,000 m^2

Groundwater contribution to carbon flux was calculated by dividing the groundwater export (Table 6) by the estuary export flux. {i.e. groundwater contribution to DIC export: 687 mmol m^{-2} of estuary d^{-1} / (35.8×10^7 mmol d^{-1} / 116160 m^2)}

940 **Table 5.** Previous studies estimating DIC and DOC export (yield) to coastal waters from small and large estuaries.
941 Units are mmol C m^{-2} of catchment d^{-1}.

Location	Description	Country	Catchment size (km^2)	DIC export	DOC export	Reference
Hat Head	Tidal estuary	Australia	18	19.8	8.5	This study (2015)
Duplin River, on Sapelo Island	Marsh-dominated estuary	USA	2	24.9*		Wang and Cai (2004)
Southwest Florida coast	Mangrove-dominated estuary	USA	230		41.1	Bergamaschi et al. (2012)
Southern Moreton Bay	Mangrove-dominated estuary	Australia	0.4	250.0	25.0	Maher et al. (2013a)
Average from different mangrove systems	Micro-tidal mangrove	USA			16.7	Adame and Lovelock (2011)
York River estuary - Chesapeake Bay	River estuary	USA	4	0.67		Raymond et. al. (2000)
Swartkops estuary	Salt marsh estuary	South Africa	4	247.3	23.5	Winter et al. (1996)
Jiulong River estuary	River estuary	China	71	2.4 - 3.9		Wang et al. (2015)
Range of different mangrove systems	Mangrove estuaries		1,992	254.0	34.2	Bouillon et al. (2008)
Chena River, Alaska	River	USA	5,200	0.9	0.3	Cai et al. (2008)
Guadalquivir Estuary (SW Iberian Peninsula)	River estuary	Spain	58,000	0.2		de la Paz et al. (2007)
Gulf of Trieste (North Adriatic)	River	Italy	500	5.0		Tamse et al. (2014)
Yukon River	River	Canada-USA	853,300	0.5-1.7	0.25-0.4	Striegl et al . (2007)
6 Arctic rivers	River	Europe	10,900,000	0.35-1.2		Tank et al. (2012)

942

943 **Table 6.** Previous studies estimating groundwater derived DIC, DOC, TAlk and CH_4 using natural tracers. Units are
944 in mmol m^{-2} of estuary d^{-1}. Table updated from Atkins et al. (2013).

Location	System description	GW-Derived DIC fluxes	GW-Derived DOC fluxes	GW-Derived TAlk fluxes	GW-Derived CH_4 fluxes	GW trancing method	Reference
Hat Head, Australia	Tidal estuary	687.3	540.2	128.1	12.5	Ra isotopes	This study (2015)
Jiulong River estuary, China	River estuary	121-897		91-748		Ra isotopes	Wang et al. (2015)
Moreton Bay, Australia	Embayment	153	36	161		Ra isotopes	Stewart et al. (2015)
Wadden Sea, Germany	Tidal flats		42	1344		^{222}Rn	Santos et al. (2015)
Heron Island, Australia	Coral reef				0.01	^{222}Rn	O'Reilly et al. (2015)
Okatee Estuary, USA	Salt marsh/estuary	1079	64		0.8	Ra isotopes	Porubsky et al (2014)
North Creek, Australia	Fresh water tidal creek	1810				^{222}Rn	Atkins et al. (2013)
Moreton Bay, Australia	Mangrove tidal creek	250	24			^{222}Rn & $\delta^{13}C$	Maher et al. (2013)
Heron Island, Australia	Permeable carbonate sediments	1.6-18.8		5.1-8.8		^{222}Rn	Cyronak et al. (2013)
Yarra River, Australia	Salt wedge estuary	349	21			^{222}Rn	Santos et al. (2012a)
Indian River Lagoon, USA	Coastal lagoon	120 - 340				$\delta^{13}C$ and $\delta^{14}C$	Dorsett et al. (2011)
West coast of Florida, USA	Sandy beach		19 - 27			Ra isotopes	Santos et al. (2009)
Okatee Estuary, USA	Salt marsh/estuary	1963	170			Ra isotopes	Moore et al. (2006)
North Inlet, USA	Salt marsh/estuary	171				Ra isotopes	Cai et al. (2003)
South Carolina, USA	Tidal creek		50			Piezometer	Goni and Gardner (2003)

945
946

947 **Figure 1**

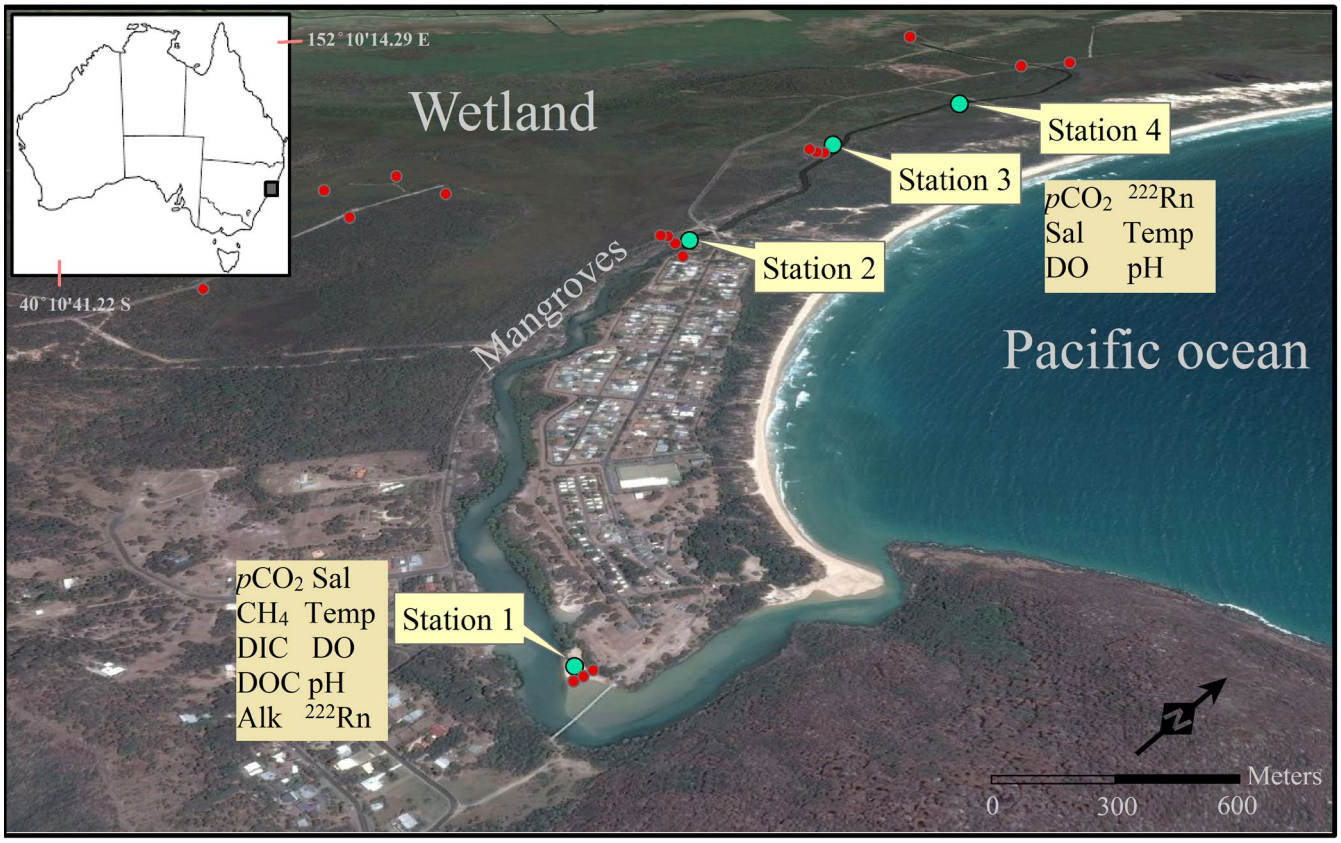

948
949

950 **Figure 2**

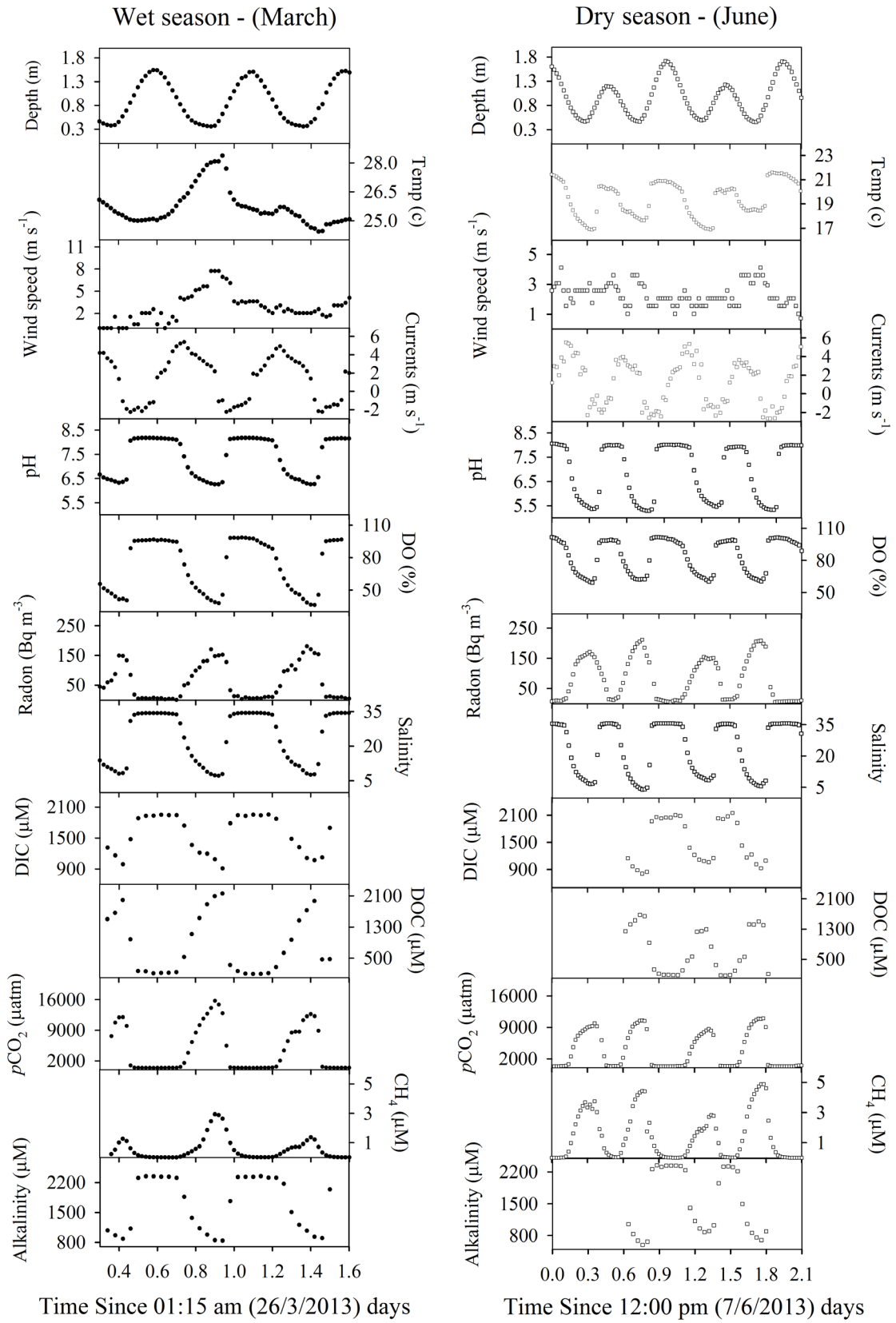

951
952

953 **Figure 3**

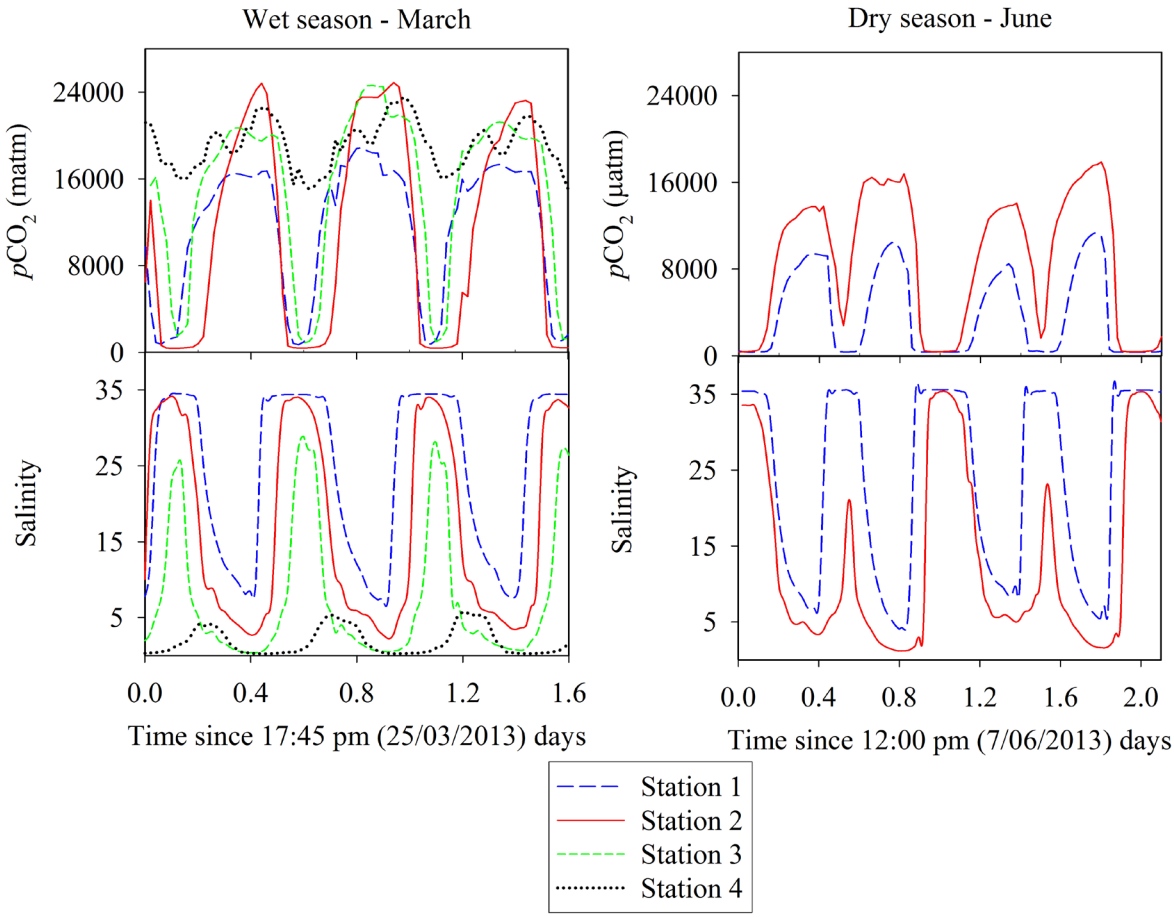

954

955 **Figure 4**

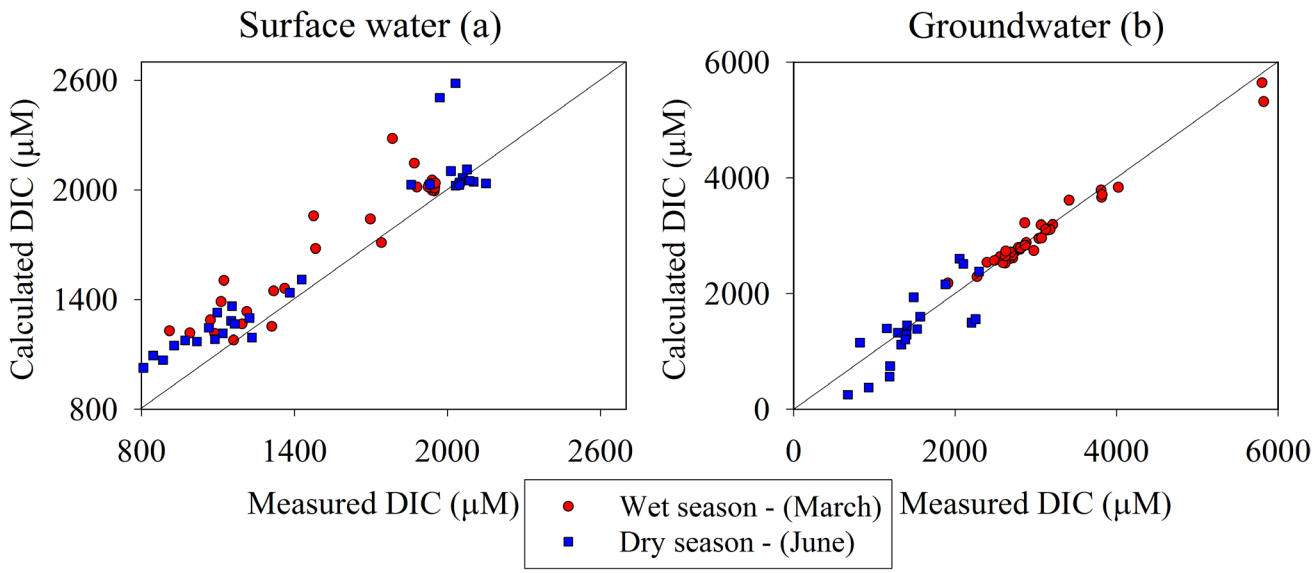

956

957

958 **Figure 5**

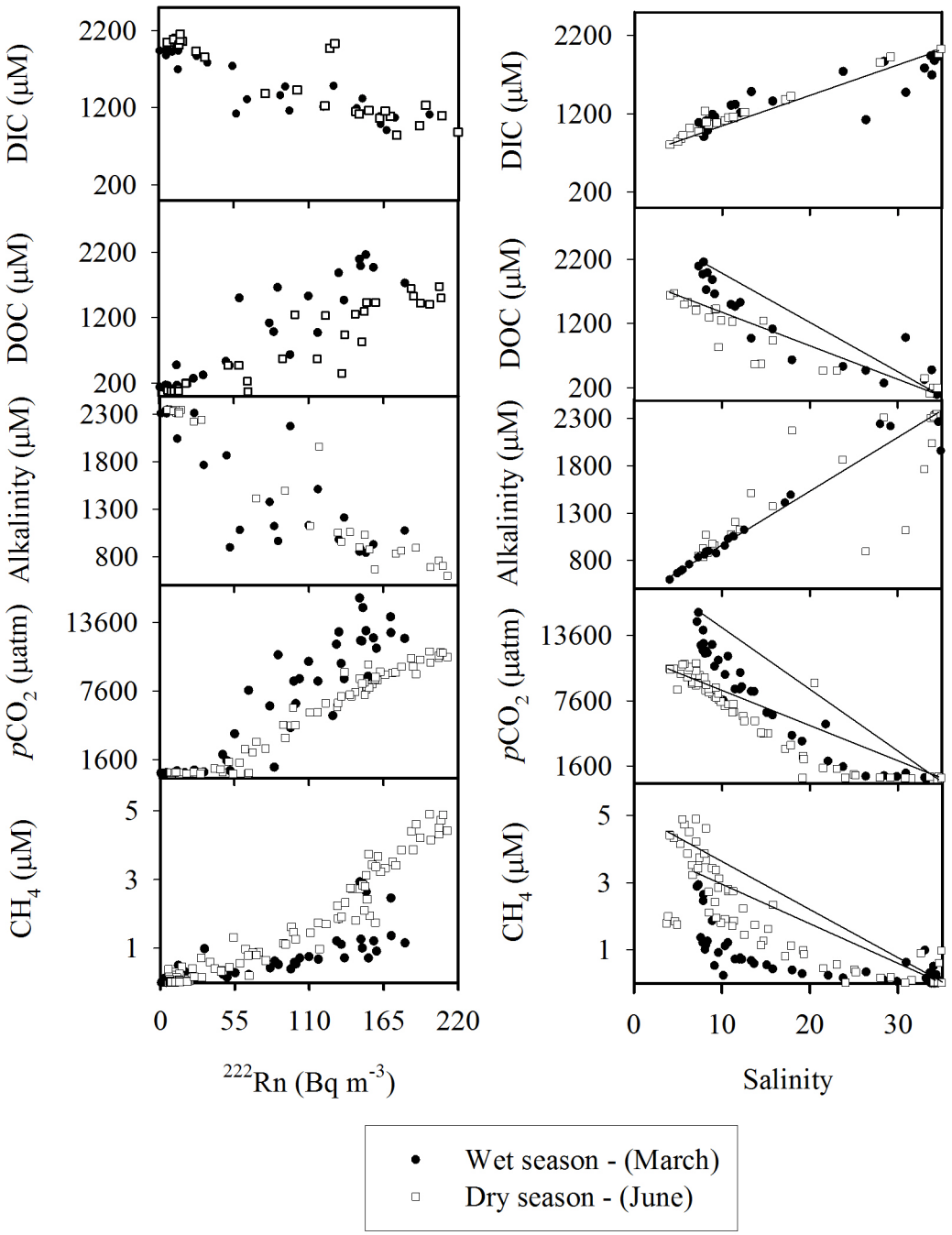

959

960

961 **Figure 6**

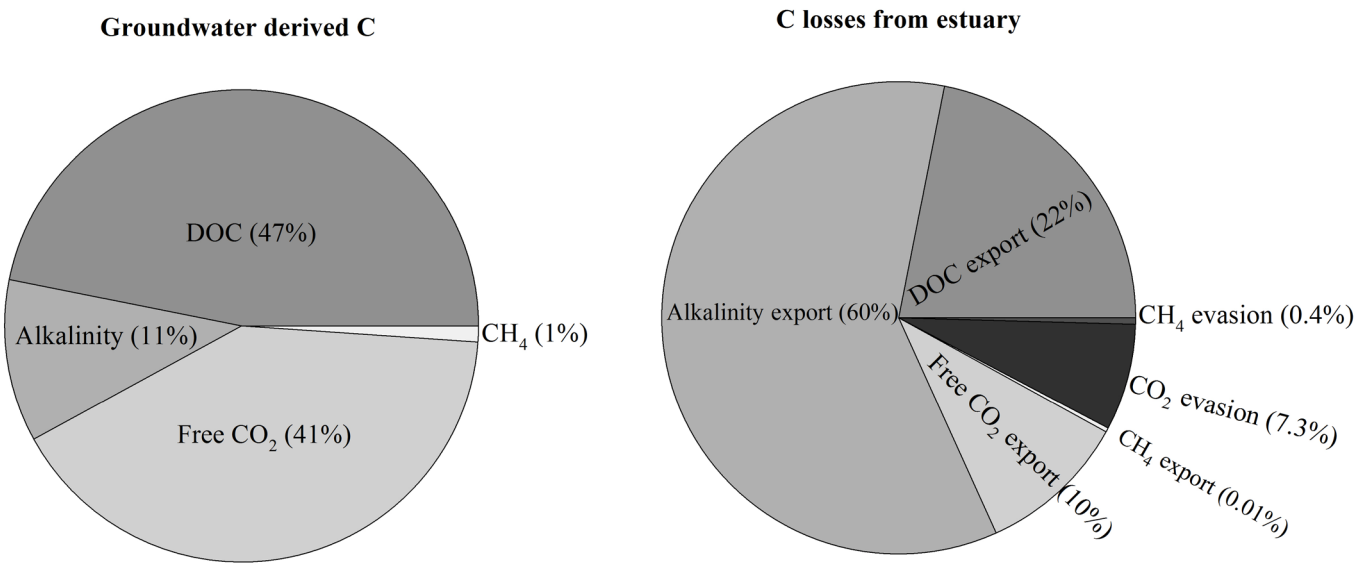

962

963

964 **Figure 7**

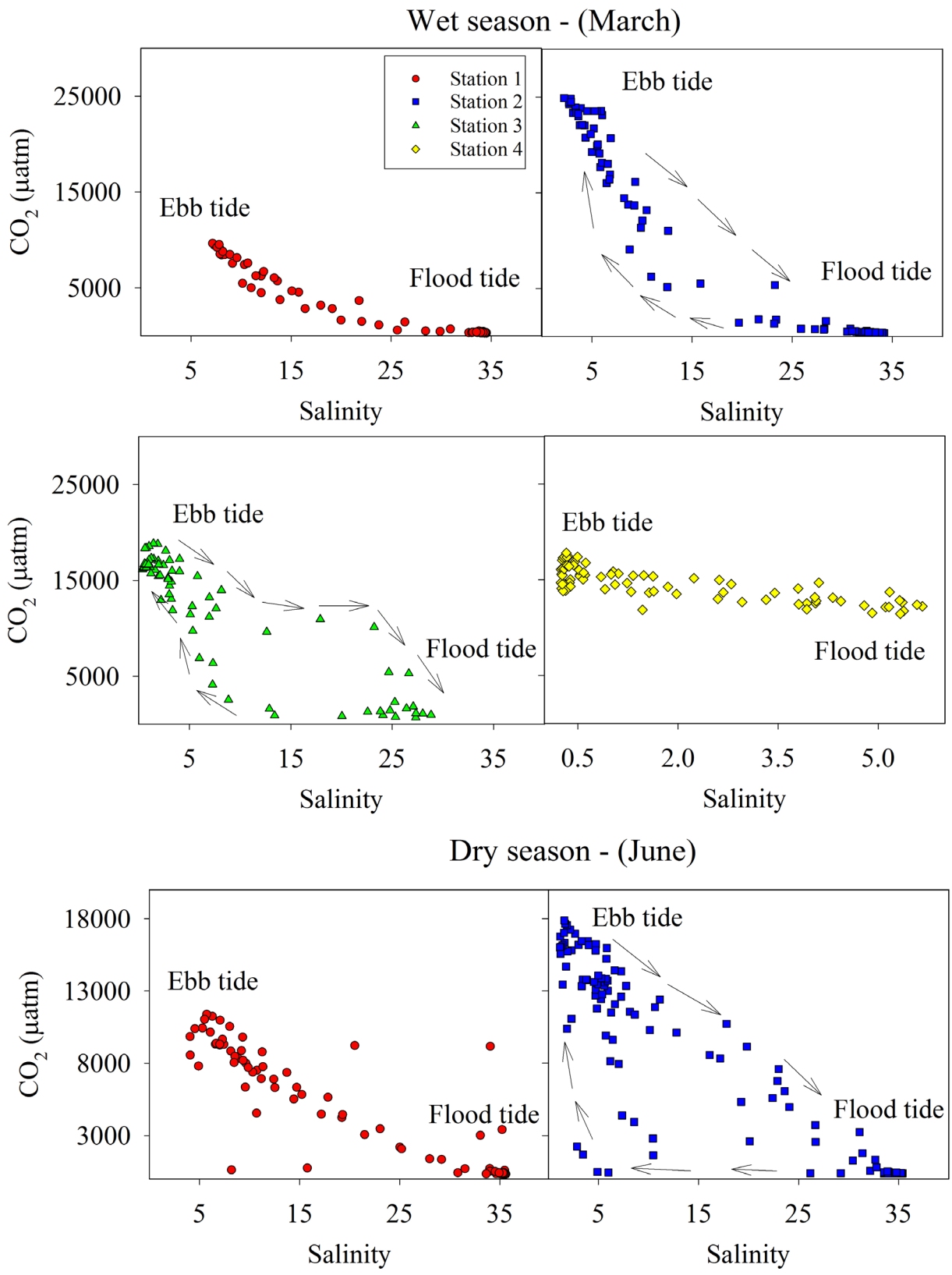

965

966

967 **Figure 8**

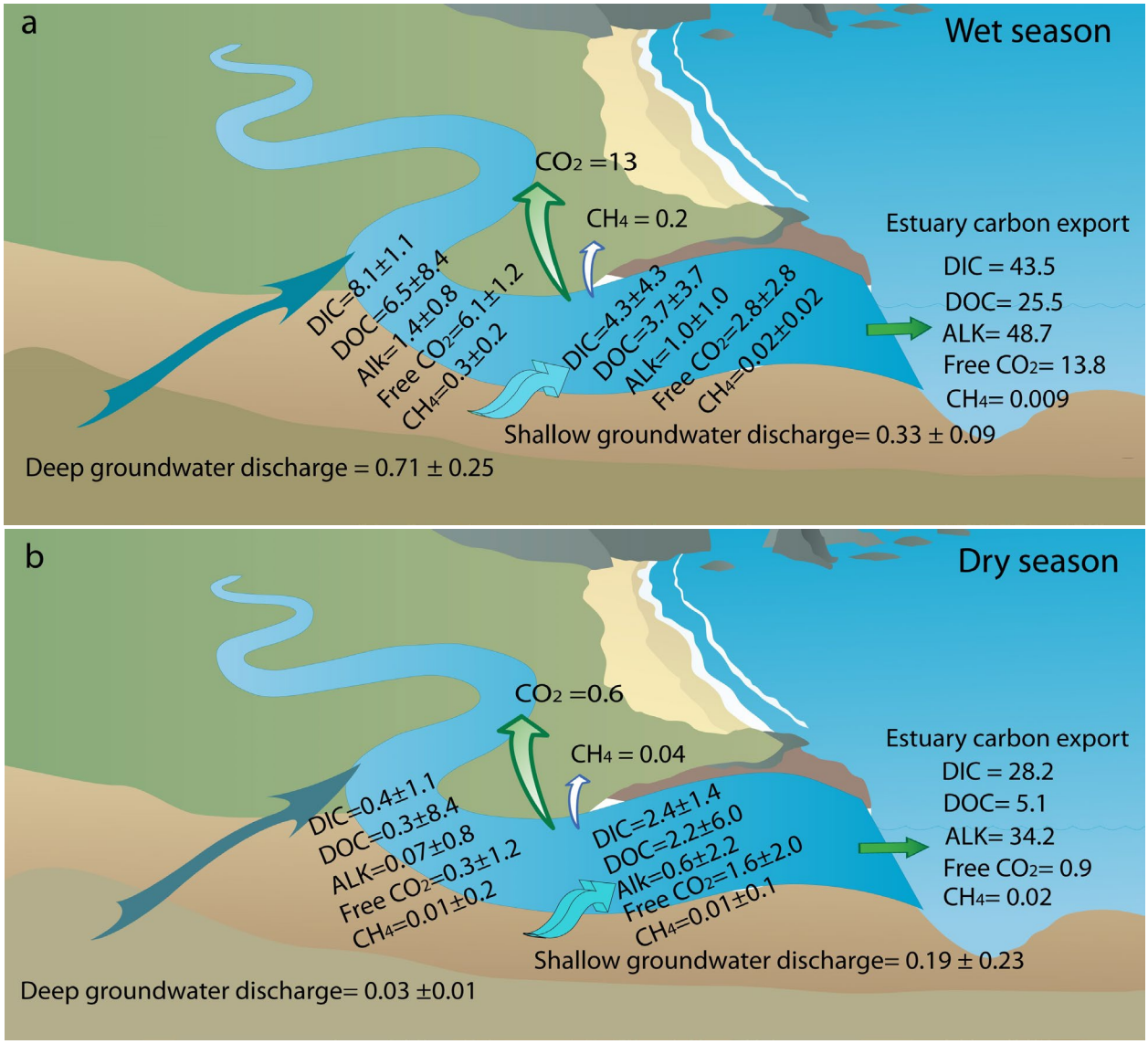

968